Under consideration for publication in J. Fluid Mech.

Numerical and Laboratory Investigation of Breaking of Steep Two-Dimensional Waves in Deep Water

ALEXANDER V. BABANIN[1], DMITRY CHALIKOV[2]
IAN R. YOUNG[1] AND IVAN SAVELYEV[3]

[1]Swinburne University of Technology, Melbourne, Victoria 3140, Australia
[2]P.P. Shirshov Institute of Oceanology, Saint-Petersburg, Russia
[3]RSMAS, University of Miami, FL 33149, USA

(Received ?? and in revised form ??)

The paper extends pilot study by Babanin *et al.* (2007a) into a detailed investigation of properties of breaking waves and processes responsible for breaking. Simulations of evolution of steep-to-very-steep waves to the point of breaking are undertaken by means of the fully-nonlinear Chalikov-Sheinin model (Chalikov & Sheinin 2005). Particular attention is paid to evolution of nonlinear wave properties, such as steepness, skewness and asymmetry, in the physical, rather than Fourier space, and to their interplay leading to the onset of breaking. The role of superimposed wind is also investigated. Instantaneously, the capacity of the wind to affect the breaking onset is minimal unless the wind forcing is very strong. Wind is, however, important on longer time scales in increasing the wave steepness and ultimately altering the breaking statistics.

Detailed laboratory study is subsequently described. The theoretical predictions are verified and quantified. In addition, some features of the nonlinear development not revealed by the model (i.e. reduction of the wave period which further promotes an increase in steepness prior to breaking) are investigated. Physical properties of the incipient breaker are measured and examined, as well as characteristics of waves both preceding and following the breaker. The experiments were performed both with and without a superimposed wind, the role of which is also investigated.

Since these idealised two-dimensional results are ultimately intended for field applications, tentative comparisons with known field data are considered. Limitations which the modulational-instability mechanism can encounter in real broad-band three-dimensional environments are highlighted. Also, substantial examination of existing methods of breaking onset detection are discussed and inconsistencies of existing measurements of breaking rates are pointed out.

1. Introduction

The breaking of deep-water surface waves represents one of the most interesting and most challenging problems of fluid mechanics. Such breaking is a strongly nonlinear intermittent random process, very rapid compared to other processes in the system of surface waves in general and wind-generated waves in particular. The distribution of breaking on the water surface is not continuous, but its role in maintaining the energy balance within the continuous wind-wave field is critical. Despite the significant research

effort devoted to the subject in the past decades, a compelling physical understanding and mathematical description of the phenomenon remain elusive.

Ocean wave breaking plays the primary role in air-sea exchange of momentum, mass and heat, and constitutes the major element of one of the most significant mechanisms which drive wave evolution - wave energy dissipation. It is also of importance for ocean remote sensing, coastal and maritime engineering, navigation and other practical applications.

In this paper, we will be mostly interested in hydrodynamic rather than air-sea interaction aspects of wave breaking. Whilst important for a variety of air-sea interaction processes, breaking is obviously mainly due to processes in the water rather than in the air. Waves are known to break even in the total absence of wind forcing, provided hydrodynamic conditions are appropriate (e.g. Melville 1982; Rapp & Melville 1990; Babanin *et al.* 2007a). Why and when will such breaking occur? Breaking waves are not only steep but have been found to also exhibit such distinct features as vertical and horizontal asymmetries (e.g. Caulliez 2002; Young & Babanin 2006), some of which cannot be reproduced by perturbation theories. Therefore, fully nonlinear theories have to be employed in the search for mechanisms leading to breaking onset.

Beyond the point of onset, breaking occurs very rapidly, lasting only a fraction of the wave period (Rapp & Melville 1990), but the wave may lose more than a half of its height (Liu & Babanin 2004). Thus, the wave energy that slowly accumulated under wind action and through weak nonlinear transfer over hundreds of wave periods is suddenly released in the space of less than one period. Obviously, this process, the breaking-in-progress process of wave collapse, is also a highly nonlinear mechanism. Conceptually, however, it is different from the processes leading to breaking onset and should be considered separately. It will not be the focus of the present paper.

Apart from the nonlinearity and the rate of energy change, intermittency is a distinct difference between breaking and other processes involved in wave evolution. Not every wave breaks whereas every wave experiences continuous energy input from the wind and continuous nonlinear energy exchange with other components of the continuous wave spectrum. It is only under very strong winds that the percentage of breaking crests in a time series can reach 50% or more. Normally it is well below 10% (Babanin *et al.* 2001). This means that on average it is only every 20th or even every 50th wave in a train that breaks. This intermittent process is, however, still sufficient to balance the continuous process of wind input and nonlinear evolution.

As stated above, breaking is primarily a hydrodynamic process. It is important to mention, however, that the three major processes which control wave evolution in field conditions: i.e. wind energy input, energy redistribution due to resonant nonlinear interactions and energy dissipation because of breaking – are closely coupled, and do affect each other. While the effect of a breaking event on the instantaneous wind input can be very significant (Babanin *et al.* 2007b), the very large density difference between the air and the water means that instantaneously the wind can only play a minor role in determining breaking onset and the subsequent breaking progress. On a longer time scale, however, the role of the wind is very important in increasing, albeit slowly, wave steepness (nonlinearity) which can then lead to wave breaking. The wind also appears to play a role in altering wave modulation properties and subsequent energy loss due to wave breaking. These multiple roles of wind forcing will also be investigated in the paper.

This paper extends our pilot numerical/laboratory study of wave breaking onset (Babanin *et al.* 2007a). As outlined in Babanin *et al.* (2007a), the topic is not new and over the last 30 years, theoretical (e.g. Longuet-Higgins & Cokelet 1978), experimental (e.g. Melville 1982) and numerical (e.g. Dold & Peregrine 1986) approaches have been applied

to investigate instability mechanisms active in nonlinear wave fields, which lead to wave breaking. These mechanisms relate to the Benjamin-Feir-like (BF) instability (Benjamin & Feir 1967) which controls the modulation of trains of weakly nonlinear waves, and as a result, some waves can become very large and ultimately break (e.g. Chalikov 2007).

In this regard, the significant conceptual difference between the current paper and most of the previous research is that this study is done in terms of free-surface wave properties in physical rather than Fourier space. We do not rely on existence of wave groups (side bands) in the initial wave field because the formation of the appropriate wave groups accompanying wave breaking is an internal process in the nonlinear wave field subject to physical instabilities. Rather, our initial conditions consist of steep monochromatic waves which are allowed to evolve naturally and this evolution appears to inevitably lead to breaking if the initial waves are sufficiently steep. Sidebands naturally grow from the background noise and are expected to be defined by the ratio of characteristic wave steepness $\epsilon = ak_0$ to spectral bandwidth $\Delta\omega/\omega_0$, where k_0 and ω_0 are some characteristic wavenumber and angular frequency respectively, and a is the mean amplitude at this wavenumber:

$$M_I = \frac{\epsilon}{\Delta\omega/\omega_0}. \tag{1.1}$$

This ratio was shown important in the original studies of instabilities of weakly modulated trains of monochromatic carrier waves of small amplitudes. Here, we denote this ratio as M_I (Modulational Index). Our study mainly deals with slowly modulated two-dimensional monochromatic waves, which are, however, even initially not of the small amplitude, and therefore, analogy of the observed empirical modulational interplay with the small-amplitude near-monochromatic theoretical BF process should be treated with caution. In our paper, M_I signifies the fact that the wave steepness and length of wave modulation (or number N of waves in the modulation where $1/N \sim \Delta k/k_0$) are not independent quantities, i.e. steeper waves will correspond to fewer waves in a modulation. Thus, if nonlinear waves are allowed to evolve naturally, they will form groups where N is not a free parameter, but will be defined by the initial steepness ϵ.

In Babanin *et al.* (2007a), prediction of the breaking onset of two-dimensional waves in deep water was attempted first by means of a fully nonlinear numerical model and then tested in a laboratory experiment. Distance to the point of breaking could be controlled by varying the Initial Monocromatic Steepness (IMS) ϵ_0. Thus, the incipient breaker was measured and found to asymptote at the Stokes steepness limit of $2\epsilon_{br} \approx 0.88$.

This paper extends the pilot study into a detailed investigation of the properties of breaking waves and the processes responsible for breaking. In Section 2 of the present paper, simulations of the evolution of steep-to-very-steep waves to the point of breaking are undertaken by means of the fully-nonlinear Chalikov-Sheinin model (Chalikov & Sheinin 2005). Particular attention is paid to the evolution of nonlinear wave properties, such as steepness, skewness and asymmetry, in the physical, rather than Fourier space, and to their interplay leading to the onset of breaking. The role of the superimposed wind is also investigated. Instantaneously, the capacity of the wind to affect the breaking onset is minimal unless the wind forcing is very strong. Wind is, however, important on longer time scales in increasing the wave steepness and ultimately altering the breaking statistics.

In Section 3, the detailed laboratory study is described. The theoretical predictions are verified and quantified. In addition, some features of the nonlinear development not revealed by the model (i.e. reduction of the wave period which further promotes an increase in steepness prior to breaking) are investigated. Since the location of the incipient breaker can be controlled, its physical properties are examined as well as characteristics

of waves both preceding and following the breaker. The experiments were performed both with and without a superimposed wind, the role of which is also investigated.

Since these idealised two-dimensional results are ultimately intended for field applications, in the Discussion Section 4 tentative comparisons with known field data are considered. Limitations which the BF mechanism can encounter in real broad-band three-dimensional environments (e.g. Brown & Jensen 2001; Onorato *et al.* 2002) are highlighted. Also, substantial examination of existing methods of breaking onset detection are discussed and the inconsistency of existing measurements of breaking rates is pointed out. Finally, overall conclusions of the study are summarised.

2. Numerical simulations

Numerical computations of nonlinear surface waves have previously been undertaken based on solutions of the potential flow equations (e.g. Watson & West 1975; Longuet-Higgins & Cokelet 1976; West *et al.* 1987) and with a Cauchy-type integral algorithm (Dold 1992). Both schemes have no limitation in terms of wave steepness, and both were capable of simulating the initial phase of wave breaking (the later stages are rotational and remain extremely difficult to simulate directly). More recently, a method based on a Taylor expansion of the Dirichlet-Neumann operator was developed by Craig & Sulem (1993). Capabilities of this method were illustrated by computing the evolution of modulated wave packets and a low-order approximation of a Stokes wave for relatively short periods of time. We should point out that this appears to be a principle limitation of all the above schemes: for a steep wave field, they have only been used for simulations of relatively short time/space evolution.

A numerical scheme for direct hydrodynamical modelling of 1D nonlinear gravity and gravity-capillary waves was developed by Chalikov & Sheinin (1998)(see also Chalikov & Sheinin 2005; Chalikov 2005, 2007). This approach is based on a nonstationary conformal mapping, which allows the equations of potential flow with the inclusion of a free surface to be written in a surface-following coordinate system. This transformation does not impose any restrictions on the shape of the surface, except that it has to be possible to represent this surface in terms of a Fourier series.

Let us consider periodic one-dimensional deep-water waves whose dynamics is described by principal potential equations. Due to the periodicity condition, the conformal mapping for infinite depth can be represented by the Fourier series (see details in Chalikov & Sheinin 1998, 2005):

$$x = \xi + \sum_{-M \leqslant k < M, k \neq 0} \eta_{-k}(\tau) exp(k\zeta) \vartheta_k(\xi), \tag{2.1}$$

$$z = \zeta + \sum_{-M \leqslant k < M, k \neq 0} \eta_k(\tau) exp(k\zeta) \vartheta_k(\xi); \tag{2.2}$$

where x and z are Cartesian coordinates, ξ and ζ a conformal surface-following coordinates, τ is time, η_k are coefficients of the Fourier expansion of free surface $\eta(\zeta, \tau)$ with respect to the new horisontal coordinate ζ:

$$\eta(\zeta, \tau) = h(x(\zeta, \xi = 0, \tau), t = \tau) = \sum_{-M \leqslant k \leqslant M} \eta_k(\tau) \vartheta_k(\zeta), \tag{2.3}$$

ϑ_k denotes the functions

$$\vartheta_k(\xi) = \begin{cases} \cos k\xi & \text{for } k \geqslant 0, \\ \sin k\xi & \text{for } k < 0 \end{cases} \tag{2.4}$$

and M is truncation number.

Nontraditional presentation of the Fourier Transform with the definition (2.4) is, in fact, more convenient for computations with real numbers, such as $(\vartheta_k)_\xi = k\vartheta_{-k}$ and $\sum(A_k\vartheta_k)_\xi = -\sum kA_{-k}\vartheta_k$. So, the Fourier coefficients A_k form a real array $A(-M:M)$, thus making possible a compact programming in Fortran90. Such presentation can be generalised for 2D case.

Note that the definition of both coordinates ξ and ζ is based on Fourier coefficients for surface elevation. It then follows from (2.1) and (2.2) that time derivatives z_τ and x_τ for Fourier components are connected by a simple relation:

$$(x_\tau)_k = \begin{cases} -(z_\tau)_{-k} & \text{for } k > 0, \\ (z_\tau)_k & \text{for } k < 0. \end{cases} \tag{2.5}$$

Due to conformity, the Laplace equation retains its form in (ξ, ζ) coordinates. It is shown in Chalikov & Sheinin (1998, 2005) that the potential wave equations can be represented in the new coordinates as follows:

$$\Phi_{\xi\xi} + \Phi_{\zeta\zeta} = 0, \tag{2.6}$$

$$z_\tau = x_\xi G + z_\zeta F, \tag{2.7}$$

$$\Phi_\tau = F\Phi_\xi - \frac{1}{2}J^{-1}(\Phi_\xi^2 - \Phi_\zeta^2) - z, \tag{2.8}$$

where (2.7) and (2.8) are written for the surface $\zeta = 0$ (so that $z = \eta$, i.e. the surface elevation), J is the Jacobian of the transformation:

$$J = x_\xi^2 + z_\xi^2 = x_\zeta^2 + z_\zeta^2, \tag{2.9}$$

G is an auxuliary function:

$$G = (J^{-1}\Phi_\zeta)_{\zeta=0}, \tag{2.10}$$

and F is a generalisation of the Hilbert transform of G, which for $k \neq 0$ may be defined in Fourier space as

$$G_k = \begin{cases} -F_{-k} & \text{for } k > 0, \\ F_k & \text{for } k < 0, \end{cases} \tag{2.11}$$

actually following from (2.5). Above, Φ is the velocity potential (and Φ_ζ is the derivative of the potential with respect to the 'vertical' coordinate ζ at the surface), z represents the shape of the surface.

Equations (2.6) – (2.11) are written in non-dimensional form with the following scales: length L, where $2\pi/L$ is the (dimensional) horisontal wavenumber, time $L^{1/2}g^{-1/2}$ and the velocity potential $L^{3/2}g^{-1/2}$ (g is the acceleration of gravity). Capillar effects and external pressure were not taken into account in this investigaion. Note that the adiabatic equations for surface waves outside the capillary interval are self-similar: they are invariant over length scale L, what makes the numerical approach very effective and allows for broad interpretations of laboratory experiments.

The boundary condition assumes vanishing vertical velocity at infinite depth

$$\Phi_\zeta(\xi, \zeta \to -\infty, \tau) = 0. \tag{2.12}$$

Solution of the Laplace equation (2.6) with boundary condition (2.12) yields to Fourier expansion which reduces the system (2.6) – (2.8) to a 1D problem:

$$\Phi = \sum_{-M \leqslant k \leqslant M} \phi_k(\tau) exp(k\zeta)\vartheta_k(\xi), \tag{2.13}$$

where ϕ_k are Fourier coefficients of the surface potential $\Phi(\xi, \zeta = 0, \tau)$. Eqs. (2.6) – (2.8), (2.10) and (2.11) constitute a closed system of prognostic equations for the surface functions $z(\xi, \zeta = 0, \tau) = \eta(\xi, \tau)$ and the surface velocity potential $\Phi(\xi, \zeta = 0, \tau)$. For more detailed descriptions of the analytical and numerical model, we refer to Chalikov & Sheinin (1998, 2005).

Remarkably, this new formulation is also simpler than the original set of equations since the nonlinear conformal coordinate transformation removes a number of nonlinear terms. For the stationary case, this method coincides with the classical complex variable method, e.g. Crapper (1957), and an efficient numerical scheme (CS) for this was developed by Chalikov & Sheinin (1998). Note that this scheme is more precise than the popular surface integral scheme (Dold 1992). In addition, compared to the CS scheme, the surface integral method is too complicated: a complete set of its equations occupy several pages. For the CS scheme, the equations take 3 lines and the core of the numeric scheme takes 11 lines in Fortran90.

The accuracy of this scheme was demonstrated by a long-term simulation of very steep Stokes waves ($ak = 0.42$). The stability of Stokes waves has been a subject of significant speculations. The reality is quite simple: Stokes waves are always unstable to any disturbances, but the rate of development of the instability depends on the amplitudes of the perturbations and their phases. In general terms, a Stokes wave is always unstable if it has any perturbation from the pure Stokes form. In the CS case, 11 decimal places of precision and a 4th order Runge-Kutta scheme were sufficient to simulate the propagation of a virtually undisturbed Stokes wave for up to one thousand periods.

The conformal mapping even made it possible to reproduce the initial stages of the breaking process where the surface ceases to be a single-valued function. Thus, the CS scheme has a number of important advantages: (1) comparison with an exact solution showed that the scheme has extremely high accuracy; (2) it preserves integral invariants; (3) it is very efficient: its computation time scales as $Mlog(M)$ where M is the number of modes, whereas the Dold scheme scales as as M^2; (4) the scheme demonstrates stability over millions of time steps (thousands of periods of the dominant wave). This scheme is able to reproduce a nonlinear concentration of energy in physical space resulting in wave breaking and potentially in the appearance of freak waves.

In the CS model, the wave model is coupled with an atmospheric boundary layer model. In the present investigation, in order to speed up the computations, the coupling was conducted by means of a β-function which parameterised the connection of the surface pressure and the surface shape on the basis of an exhaustive set of numerical simulations by means of the coupled model. The real and imaginary parts of this β-function are functions of non-dimensional frequency. Thus, it is possible to introduce wind forcing of the waves. This option will be actively employed in this study.

2.1. *Testing the Chalikov-Sheinin model*

For the purposes of the present study, the model's ability to reproduce wave evolution without limitations in terms of steepness or duration of propagation is crucial. For this reason, the CS model was chosen for the detailed numerical simulations of physical characteristics of strongly nonlinear waves leading to the onset of breaking. Before being employed in the present study, the CS model had previously been extensively verified and tested (Chalikov & Sheinin 1998, 2005) and used in a number of strongly nonlinear applications (e.g. Chalikov 2005, 2007). It was now additionally checked in terms of its capacity to model nonlinear wave features associated with wave breaking.

One of early motivations for the present study was to search for a theory able to describe wave asymmetry with respect to the vertical axis. Definitions of the asymmetry

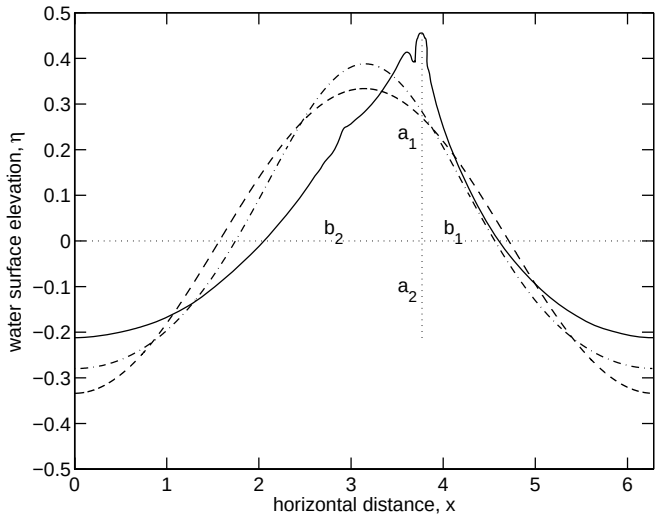

FIGURE 1. Geometric definition of wave skewness and asymmetry. The wave propagates from left to right. b_1 and b_2 are horizontal distances from the breaker crests to the zero-downcrossing and -upcrossing respectively. a_1 and a_2 are the breaker crest height and trough depth respectively. Solid line - numerically simulated incipient breaker. Dashed line - harmonic wave of the same wavelength and wave height. Dash-dotted line - Stokes wave of the same length and height. Dotted lines are the mean (zero) water level (horizontal) and the line drawn from the breaker crest down to the level of its trough (vertical).

and skewness (asymmetry with respect to the horisontal axis) are given in figure 1, reproduced with modifications from Babanin *et al.* (2007a). In mathematical terms, these definitions are:

$$A_s = \frac{b_1}{b_2} - 1; S_k = \frac{a_1}{a_2} - 1. \tag{2.14}$$

Thus, positive skewness represents a wave with a crest height greater than the trough depth and negative asymmetry represents a wave tilted forward in the direction of propagation.

Intrinsically, both the asymmetry and the skewness are natural features of steep deep-water waves regardless of their size, crest length, forcing or generation source. Importantly for this study, experimentally observed asymmetry A_s has been broadly associated with the wave breaking (e.g. Caulliez 2002; Young & Babanin 2006). Perturbation theories, being essentially spectral theories, cannot reproduce such asymmetry for deep-water waves, and therefore, since we intended to study physical features of near-breaking waves, a fully-nonlinear theory was obviously required. Figure 1 illustrates the capacity of the CS model in this regard. In the figure, three types of waves of the same height and length, i.e. of the same mean steepness, are shown. Once the skewness is non-zero and the amplitude a is not clearly defined, a definition of the wave steepness in terms of ak becomes ambiguous. Therefore, unless otherwise specified, the steepness will be expressed in terms of wave height $H = a_1 + a_2$ rather than wave amplitude a, as $\epsilon = Hk/2$. In these terms, a steepness $\epsilon = 0.335$ of the wave shown in the figure far exceeds the limits of a perturbation analysis.

The dashed line in figure 1 represents a steep sinusoidal wave ($S_k = A_s = 0$). Such a wave will immediately transform itself into a Stokes wave (e.g. Chalikov & Sheinin 2005),

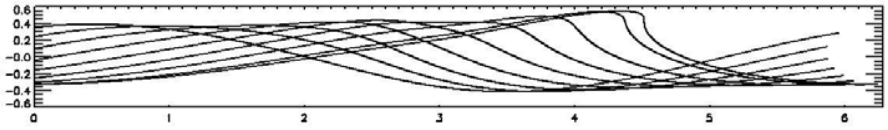

FIGURE 2. Numerical simulation of a steep wave developing asymmetry, as predicted by the CS model. The wave propagates from left to right. The ratio of horisontal and vertical scales is 1.

an example of which is shown in the figure by the dash-dotted line. This steep Stokes wave is highly skewed ($S_k = 0.39$), but remains symmetric (i.e. $A_s = 0$). The incipient breaker in figure 1 (solid line, $S_k = 1.15, A_s = -0.51$) was produced by the CS model, in a simulation which commenced with an initially monochromatic wave of $IMS = 0.25$ (Initial Monochromatic Steepness). Such a wave profile visually looks realistic for a breaker and corresponds to, or even exceeds, experimental values of skewness and asymmetry for breaking waves previously observed (e.g. up to $A_s = -0.5$ instantaneously in Caulliez (2002) or $A_s = -0.2$ on average in Young & Babanin (2006)). It is worth noting that the steepness of the individual wave has grown very significantly at the point of the breaking: from $IMS = 0.25$ to $\epsilon = 0.335$. Result shown in figure 1 was obtained for initially assigned harmonic wave at wave number $k = 1$ and number of modes $M = 1024$. All other computations described below were conducted for an harmonic wave assigned at $k = 16$ and number of modes $M = 2048$.

Disturbance seen at the crest of the incipient breaker in figure 1 has to be mentioned. For waves of very high steepness, instabilities of the local flow near wave crest, which are different from instabilities of the whole wave, are known to develop (e.g. Longuet-Higgins & Dommermuth 1997). Disturbance seen in figure 1 appears to be due to an instability of this kind - i.e. crest instability. Such instabilities, i.e. the crest instabilities of the waves approaching the limiting steepness, is a large topic in its own right and a topic different to the modulational instability of waves which leads to the growth of very high waves and ultimately to the breaking and accompanying crest instabilities. This topic will not be discussed in the present paper.

The capacity of the CS model is further demonstrated in figure 2. Here, the rapid growth of asymmetry A_s of a very steep harmonic wave with steepness $\epsilon = ak = 0.32$ is shown in terms of dimensionless time (in the horizontal scale, 2π corresponds to the wave period). This is effectively a developing breaker, as in the two-dimensional CS model such waves break within one period (see figure 6 below).

2.2. *Simulating the evolution of nonlinear waves to breaking*

In numerical simulations of the fully nonlinear evolution of steep two-dimensional waves to the point of breaking, we will concentrate on three physical properties: wave steepness, skewness and asymmetry, and their inter-relationships. We will then try to reproduce and investigate these properties in a laboratory experiment with two-dimensional waves. If these properties are indeed linked to wave breaking, but the percentage of breaking waves is small, as it usually is (see Section 1 above), then examination of average steepness, skewness or asymmetry is likely to be of little use. Therefore, the majority of our analysis will concentrate on nonlinear properties of individual waves.

In figure 3, development of an unforced wave (no wind) to the point of breaking is shown. When modelling, a wave is regarded as breaking (simulations stop) when the water surface becomes vertical at any point. The wave shown had $IMS = 0.16$ and is regarded as moderately steep in terms of BF instability. This moderate steepness will allow a reasonably long evolution before breaking occurs. Therefore, the simulation will

produce a general, rather than detailed picture to begin with (the time scale is expressed in wave periods, i.e. the wave breaks after 82 periods).

As seen in the figure, the steepness of individual waves stays reasonably constant for a significant number of periods (∼30), before it starts oscillating noticeably. The magnitude of the oscillations increases significantly beyond the 60th period, and from this point grows rapidly until the simulation ceases (wave breaks) after the 80th period.

Similar behaviour is exhibited by the skewness and asymmetry. The simulation starts from a Stokes wave of $S_k = 0.18$ and $A_s \approx 0$. It is informative to note that prior to breaking, the magnitude of the skewness oscillation is so large that at times the wave even becomes negatively skewed, i.e. trough is deeper than crest. At the termination of the simulation, however, $S_k \approx 1$, that is the crest is twice is high as the trough (2.14). In section 3.2, it is shown that laboratory waves asymptote to this value of skewness at the onset of breaking. The asymmetry also oscillates through the simulation and reaches the experimentally observed breaking magnitude of $A_s \sim 0.5$ (i.e. Caulliez 2002).

As mentioned above, the simulations shown in figure 3 were conducted without wind forcing applied, and therefore this is the hydrodynamic instability that leads the waves to breaking. It should be noted that comparisons of such numerical simulations with experiments can only be qualitative. At the initial stages of development, the necessary BF modes, if they are absent, should grow from the continuous background noise. Such noise is suppressed in a discretised numerical model, particularly if the model is very precise.

Figure 4 shows the simulated evolution of the nonlinear wave properties to the point of breaking in the presence of wind forcing. The wind forcing is expressed in terms of ratio U/c where U is the wind speed and c is the phase speed of the wave with wavenumber k. Three sets of subplots correspond to three wind-forcing conditions: $U/c = 2.5$ (moderate forcing), $U/c = 5.0$ (strong forcing) and $U/c = 10.0$ (very strong forcing). The initial steepness chosen is $IMS = 0.26$, which should lead to a faster evolution to breaking onset. Note that the minimum value plotted on the steepness scale is $\epsilon = 0.25$ and not zero, and that the simulation starts from a harmonic wave with $S_k = A_s = 0$.

The top three panels correspond to a moderate wind-forcing condition of $U/c = 2.5$. Under such wind, it takes approximately 32 wave periods to reach the point of breaking. The period of the modulation is equal to twice the wave period, which is consistent with the theoretical expectations for BF instability (Longuet-Higgins & Cokelet 1978). With the wind forcing applied, the maxima of instantaneous steepness keep growing and reach a value of $\epsilon = 0.34$ at the point which is interpreted as incipient breaking by the model.

The skewness and asymmetry oscillate with the same double-wave period, but without a noticeable increase in magnitude of the oscillation. For example, the value of $S_k = 0.84$ of the skewness at breaking is repeatedly reached by the wave in its progress without breaking. Therefore it appears that of the parameters shown here, it is the local steepness that determines the point of breaking. Visually, skewness is in phase with the steepness oscillations, and it relaxes back to zero when the steepness is at its minimum (although the wave does not become sinusoidal again as the asymmetry is not zero at this point).

The oscillations of asymmetry are shifted in phase with respect to steepness and skewness. The asymmetry oscillates about zero in the range ± 0.45 which means that the waves are periodically tilted backward and forward. When steepness (skewness) is a maximum, asymmetry is zero, i.e. the wave is symmetric with respect to the vertical. If the point of maximum steepness (skewness) is passed without breaking, the asymmetry becomes negative. That is, the wave begins to lean forward. If this point signifies the breaking onset, the wave is apparently still continuing to tilt forward, and this explains why all the breaking waves exhibit negative asymmetry. In these simulations, the negative asym-

FIGURE 3. Numerical simulation of evolution of a wave with $IMS = 0.16$ to the point of breaking (no wind). Time scale is in wave periods. (top) wave slope (steepness where minus sign signifies the forward face slope); (middle) skewness; (bottom) asymmetry.

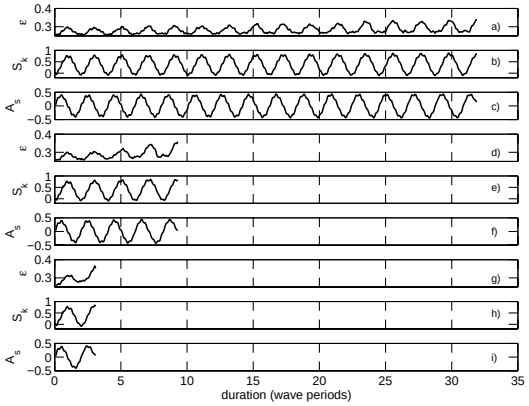

FIGURE 4. Simulations of steepness (a,d,g), skewness (b,e,h); asymmetry (c,f,i) of the wave of $IMS = 0.26$ as it evolves from the initial conditions to the point of breaking. Top three panels: $U/c = 2.5$; middle three panels: $U/c = 5.0$; bottom three panels: $U/c = 10.0$. X-label shown at the bottom is the same for all panels.

metry does not appear an indication of the breaking but is rather an indication of the modulation phase at which breaking-in-progress may or may not occur.

The second set of three panels correspond to wind forcing of $U/c = 5.0$. Such forcing is quite strong, and therefore the steepness growth rate is much faster than above. Apart from the steepness growth, almost all the other properties of the nonlinear evolution remain similar to the previous test. Steepness ($\epsilon = 0.36$) and skewness ($S_k = 0.82$) values at breaking are close to those of the above test, asymmetry at breaking approaches zero. Thus, it can again be concluded that it is some critical value of local steepness which defines the breaking onset.

It is interesting to note that, according to known results on the wave amplification by wind, the wave growth increment at non-extreme conditions should be approximately a quadratic function of the wind (e.g. Donelan *et al.* 2006). If indeed there is some critical steepness signifying the breaking onset, then doubling of the wind speed in our numerical tests should lead to this limiting value being reached four times faster. This conjecture produces a result close to that simulated: the duration of the evolution to breaking has now been reduced from 32 to 9 wave periods (almost 4 times).

A further doubling of the wind input, as shown in the bottom set of three panels, led to another reduction of the evolution duration - from 9 to 3 periods. This is again consistent with Donelan *et al.* (2006) who showed that at very strong winds the relative wave growth actually slows down. The other patterns of the wave nonlinear evolution appear unaltered. The test again indicates a critical local steepness as the parameter responsible for the onset of the water surface collapse. The maximum values of steepness $\epsilon = 0.36$ and skewness $S_k = 0.83$ are almost the same as previously. These values also demonstrate that the instantaneous effect of the wind on the breaking onset is negligible. The wind forcing of $U/c = 10.0$ is now very strong, but this wind is still not capable of pushing the wave over and reducing, even marginally, the critical steepness at breaking.

We now conduct a similar set of numerical simulations for a wave with initially half the steepness $IMS = 0.13$ (figure 5). A very strong forcing of $U/c = 10.0$ is applied in order to achieve breaking in a reasonably short period of time. The wave steepness grows under the $U/c = 10.0$ wind forcing so rapidly that its oscillations are barely visible over the strong mean trend. The value of steepness $\epsilon = 0.33$ at the point of breaking,

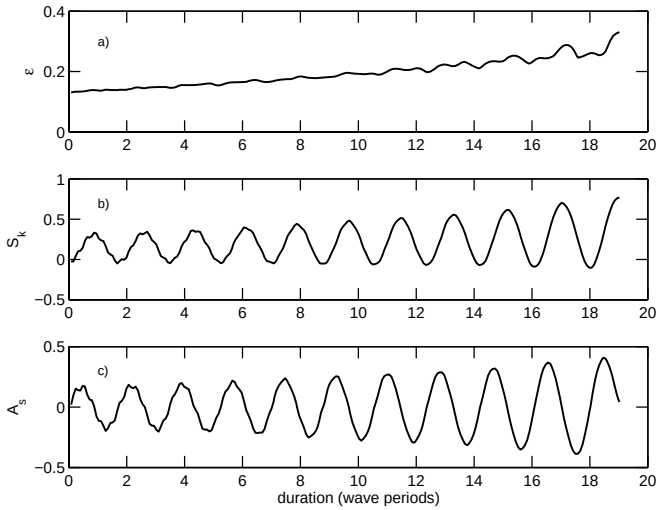

FIGURE 5. Simulations of a) steepness, b) skewness; c) asymmetry - of the wave of $IMS = 0.13, U/c = 10.0$ as it evolves to breaking.

similar to the previous tests. This again supports the concept of a limiting breaking-onset value. Compared with for the same wind forcing in figure 4, it now takes much longer (19 wave periods versus 3) to achieve this steepness, but as soon as this value of steepness is reached, the wave breaks.

It should be mentioned that the limiting steepness in the numerical simulations can only be treated in a statistical rather than in absolute sense. In individual computer runs, steepness of waves at the point where the simulations stop (i.e. the water surface becomes vertical at least in one point) is scattered. This is due to the carrying wave being distorted by nonlinear interactions with bound waves and by modulations which grow from the background noise. In the laboratory experiment described below such limiting steepness was obtained as an asymptotic value for measurements approaching the breaking onset.

It is instructive to observe the behaviour of the skewness and asymmetry of these initially much less steep waves. Since nonlinearity is now obviously weaker, the oscillations start with much smaller magnitudes of $S_k = 0.33$ and $A_s = 0.18$. They do eventually grow to maxima of $S_k = 0.77$ and $A_s = 0.41$ similar to those values observed previously. These may be indicative of limiting values of the wave skewness and asymmetry, but they are obviously not a breaking criterion as in the previous test they did not lead to breaking unless limiting steepness was also reached. Kinematics leading to the observed oscillations and limiting values of S_k and A_s is very complex and will be discussed in a separate paper.

Figure 6 shows a composite set of fetch-versus-steepness dependences for different values of wind forcing $U/c = 1-11$. The fetch is expressed in dimensionless terms of number of wavelengths (wave periods) to the breaking at a particular IMS. Dependences appear quasi-linear in the range of parameters shown, but as discussed in Babanin *et al.* (2007a), they are best approximated by the function of hyperbolic tangent. That is, waves with no superimposed wind forcing and $IMS < 0.1$ will never break, even though they will exhibit oscillations of steepness, asymmetry and skewness similar to those discussed above. Evolution of such waves is not shown in the figure, and in fact we do not plot $IMS < 0.17$ because such development to breaking is too slow for the purpose of demonstration. The

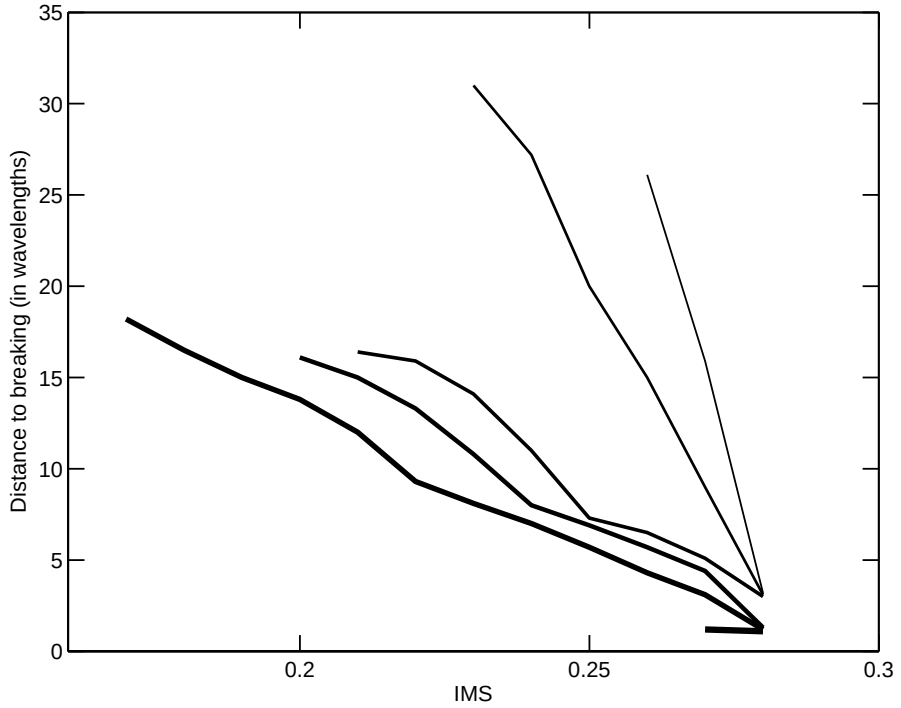

FIGURE 6. Numerical simulations, number of wavelengths to the breaking versus $IMS = ak$, different wind forcing of $U/c = 1, 3, 7.5, 8, 8.5, 11$ is shown with progressively thickening lines.

upper limit of steepness included is $IMS = 0.28$ as waves with $IMS > 0.3$ will break immediately, within one period.

Figure 6 is the most important result of Section 2. It allows the estimation, based on the numerical simulations with the CS model, of when a two-dimensional wave breaks. As has been mentioned, quantitative application of these numerical results to laboratory waves may be limited, but as it will be shown in Section 3, qualitatively this picture agrees well with experiment.

2.3. *Breaking onset*

In the numerical simulations, a wave is regarded as breaking if the water surface becomes vertical at any point. Criterion for terminating the model run was defined by the first appearance of a non-single value of surface in the interval $x = (0, L)$:

$$x(i+1) < x(i), i = 1, 2, 3..., N-1, \tag{2.15}$$

where N is the number of points on the wave profile over its length L.

Figure 7 shows simulated wave profiles prior to breaking at the point when the wave of $IMS = 0.26$ reached its maximum values of negative asymmetry (left) and skewness/steepness (right). Note that these points are separated by three quarters of the oscillation period. Nonlinear evolution of this wave has been analysed in figure 4 of section 2.2 above. As in figure 4, cases of $U/c = 2.5, 5.0$ and 10.0 are shown.

The shape of the wave on the left corresponds well to the common notion of a breaker. Its negative skewness of $A_s = -0.42$ (for all the three winds) is high by all standards (e.g. Caulliez 2002). As indicated by figure 4, however, this is not yet an incipient breaker.

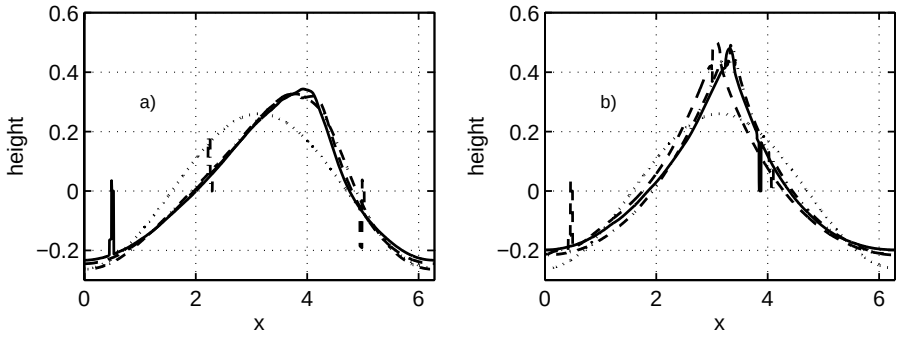

FIGURE 7. Numerically simulated wave profile prior to breaking. Waves propagate from left to right. a) minimum (maximum negative) asymmetry; b) maximum skewness/steepness. $IMS = 0.26, U/c = 2.5$ (solid line), 5.0 (dashed line), 10.0 (dash-dotted line). Initial wave is shown with dotted line.

This wave will continue to develop to the shape shown on the right which is interpreted within the model as incipient breaking. If compared with the dashed profile of the initial wave, one can see that the trough is flatter, the crest is much sharper.

Both in figure 7a and 7b, wave profiles evolved significantly from the initial harmonic wave shown by the dashed line. Despite the fact that evolution occurred under very different wind forcing conditions, and took very different times to reach the breaking point, the magnitudes of the asymmetry ($A_s = -0.42$), skewness ($S_k = 0.84, 0.82, 0.83$) and steepness ($\epsilon = 0.34, 0.36, 0.36$), as well as the profiles of the three waves, are virtually identical. This highlights again the important role of the hydrodynamic mechanism in forming the nonlinear wave profile, whereas the wind appears to serve merely as the source of energy to the wave system.

2.4. *Influence of wind and initial steepness*

The role of the wind in the wave breaking has already been mentioned. It is apparently very important in growing the wave steepness (i.e. figures 4, 5, 6). In this section, we will discuss the capacity of the wind to instantaneously affect the breaking onset. That is: can the wind push a steep wave over and thus reduce the limiting steepness at breaking?

Due to the very large density difference between the water and the air, such a possibility seems unlikely. This conjecture is supported by figures 4, 5, 7. In figure 8, the nonlinear features of the incipient breaker are shown as a function of IMS for a variety of wind-forcing conditions. Note that the simulations were run for a limited number of wave periods (i.e. a simulation was stopped after some 400 wave periods regardless of whether the wave has reached breaking onset or not). Thus, in these numerical experiments, some waves may not break (e.g. for $U/c = 3$, the waves do not have enough time to break if $IMS < 0.25$).

In figure 8a, the limiting steepness at breaking onset is plotted for $U/c = 3$ (dotted line), 5 (dashed line), 8 (dash-dotted line) and 11 (solid line). The incipient-breaking steepness actually grows, rather than being reduced, with stronger wind forcing. Even though the growth is marginal, the four lines clearly separate and therefore instantaneous steepness at breaking appears to be somewhat larger at stronger winds. The skewness and asymmetry of the incipient breakers (figure 8bc) do not depend on wind except at the extreme wind forcing of $U/c = 11$. Thus, it is only at extreme conditions that the

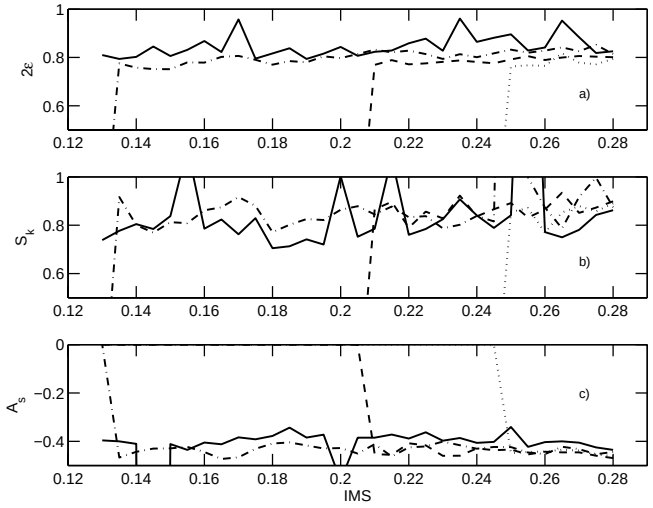

FIGURE 8. The influence of wind on the nonlinear properties of incipient breakers. a) steepness; b) skewness; c) asymmetry - versus IMS for $U/c = 3$ (dotted line), 5 (dashed line), 8 (dash-dotted line) and 11 (solid line).

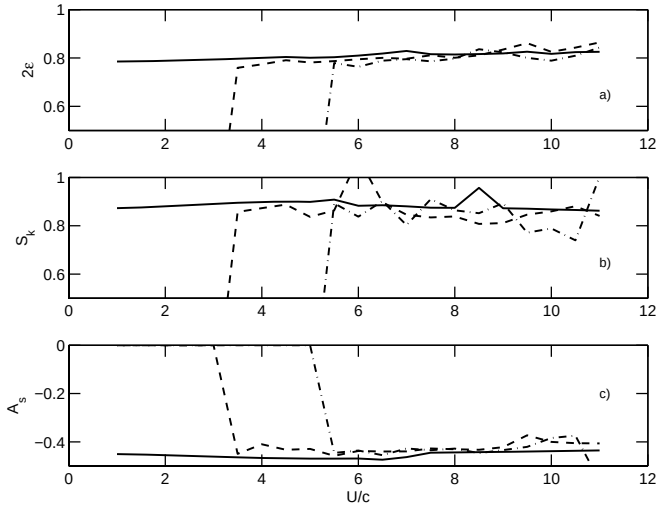

FIGURE 9. The influence of wind on the nonlinear properties of incipient breakers. a) steepness; b) skewness; c) asymmetry - versus U/c for $IMS = 0.20$ (dash-dotted line), 0.24 (dashed line) and 0.28 (solid line).

wind is capable of influencing the wave shape at breaking, and even then the effect is marginal.

The same properties of the incipient breaker are plotted versus U/c for three different IMS values of 0.20, 0.24 and 0.28 in figure 9. The value of $IMS = 0.28$ is extreme and the wave grows to the limiting steepness almost instantaneously - within $1 - 3$ periods (see figure 6). Note that the simulation was again run for a limited number of wave periods. As a result, in the case of $IMS = 0.20$, the waves do not have enough time to break if $U/c < 5$.

Apart from the mentioned above slow growth of the limiting steepness as a function of wind, the effects are weak and only noticeable when $IMS = 0.28$. Thus, the numerical simulations of the breaking onset do reveal some influences which the wind forcing and initial-steepness conditions have on the onset of breaking, but those are marginal and some can only be noticed at extreme winds and critical initial steepness.

3. Laboratory experiment

To begin this section, it should be emphasised that comparisons of the numerical simulations of nonlinear wave evolution described above with the laboratory experiments in this section can only be qualitative. Firstly, no matter how sophisticated the model is, it is still a simplification of the physical environment and disregards or possibly suppresses some natural features. One of such features is the three-dimensionality of wave motion. Even in the quasi-two-dimensional environment of the wave tank, some directional features may still play an essential role. For example, Melville (1982) showed that at steepness $\epsilon > 0.3$ the wave crests develop a crescent-shaped perturbation and such wave behaves in a more complicated way compared to the strictly 2D BF case. This has a significant consequence for our simulations. The two-dimensional CS model predicts immediate breaking onset for $\epsilon > 0.29$ whereas in the laboratory experiments of Melville (1982) such waves become short-crested but can persist without breaking for some time.

Another significant difference between the laboratory and model is the continuous nature of modes in the experimental environment, even if those modes are only minor background noise, and the discrete nature of numerical modes. It is important to understand that at the initial stages of development, the necessary modes, defined by M_I (1.1), should grow from the continuous noise. These modes, however, can be suppressed or even removed completely in a discretised numerical model. In such circumstance, the waves, even if they are steep Stokes waves, will propagate for an indefinitely long period without breaking, as was described in Section 2.

If the model is constructed so as to allow multiple modes, another numerical feature still distinguishes the model from nature. The background noise, the source of the necessary modes dictated by M_I, cannot be completely reduced to zero in nature. In a digitised medium it can, however, be made very small. For example, in the CS numeric scheme, the 11th order decimal accuracy is employed. Such accuracy is essential for precise simulations, but since it is the only source of noise in the system, it can obviously slow down the development of the initial BF modes. As is sometimes done in numerical simulations (e.g. Dold & Peregrine 1986), the modes can be deliberately introduced as initial conditions. Such an approach was not, however, employed in the present study, since in this scenario M_I of the system is pre-defined, and wave development to breaking may be altered.

A further implication of the numerical modelling, essential for the present study, has been mentioned in section 2.3 above. The model has obvious limitations in simulating the final stages of incipient breaking and was stopped when the water surface became vertical at any point. Strictly speaking, this geometrical property of the surface can be used as a physical definition of the breaking onset. In the numerical simulations it was noticed that the local steepness can be very large, but the carrier wave can still recover to a non-breaking state. If, however, a negative slope appears locally, the wave never returns to a non-breaking scenario because the water volume intersecting the vertical line tends to collapse. Apparently, the same considerations are applicable to the physical waves too.

At present, the concept of incipient breaking or breaking onset is poorly defined and

even ambiguous. Traditionally, the initial phases of a breaker-in-progress are treated as incipient breaking. As an example, let us consider how 'near-breaking' was defined in the paper by Caulliez (2002), whose investigation of the asymmetry of such near-breaking waves motivated, to some extent, the present study. In Caulliez (2002), surface elevations were recorded, differentiated, and the wave was regarded as a 'near-breaker' if its slope exceeded 0.586 anytime between two subsequent zero-downcrossings. This criterion is an estimate of the highest slope which a Stokes wave can reach (Longuet-Higgins & Fox 1977). But if this slope is exceeded, then the wave is not about to break – it is already breaking. This is not an incipient breaker, but represents breaking in progress. Features and physics of breaking-in-progress, however, may be very different to that of incipient breaking. Thus, investigation of geometric, kinematic, dynamic and other properties of breaking-in-progress, such as whitecapping, void fraction, acoustic noise emitted by bubbles etc., will be of little assistance if we are seeking to understand the causes of breaking.

In this paper, as in Babanin *et al.* (2007a), we suggest that the incipient breaker is defined dynamically as a wave which has already reached its limiting-stability state, but has not yet started the irreversible breaking process. That is, breaking onset is the ultimate point at which the wave dynamics caused by initial instabilities is still valid. This definition allows the identification of incipient breakers and, once the location of the breaking onset can be predicted, allows measurement of the physical properties of such waves. The state of breaking onset is instantaneous unlike breaking-in-progress which can be further subdivided into a number of stages with different properties and different dynamics (Liu & Babanin 2004).

3.1. *Laboratory setup*

The laboratory experiment was conducted in the Air-Sea Interaction Salt water Tank (ASIST) at RSMAS, University of Miami (http://peas.rsmas.miami.edu/groups/asist). The tank is a stainless-steel construction with a working section of 15m x 1m x 1m. Its programmable fan is capable of generating centreline wind speeds in the range of 0 to 30m/s. Immediately downstream of the fan, extensive flow straightening devices are installed to condition the air flow and introduce appropriately scaled turbulence. Values of wind speed U used in this paper will be those extrapolated to 10m height.

ASIST includes a fully programmable piston wave maker able to produce both monochromatic waves and waves with a predefined spectral form. A set of dedicated measurements showed that amplitude of the first harmonics is of the order of 1% of the amplitude of sinusoidal waves generated by the piston in the range of steepness ak between 0.25 and 0.3. These waves are dissipated at the opposite end of the facility by a minimum-reflection beach. The ASIST beach design has been a subject of a special research project. A gently-sloping (10 degrees) grid of 2.5cm diameter acrylic rods is used. A perforated acrylic plate is placed beneath the rods to split wave orbital velocities into multiple turbulent jets to increase viscous dissipation. The energy of the reflected component is approximately 5% of the incident energy depending on the initial wavelength.

In ASIST, sloshing motion becomes increasingly important at wave frequencies exceeding 2.2 Hz. For frequencies below 2Hz, the waves remain two-dimensional with phase fronts perpendicular to propagation direction. Therefore, our laboratory experiments with 2D waves were limited to frequencies below 2Hz.

In the present experiment, monochromatic deep-water two-dimensional wave trains were generated by the wave paddle. The water depth was held at 0.4m, providing deep-water conditions for the wave frequencies involved. With a tank length of 13.24m, surface elevations were recorded at 4.55m, 10.53m, 11.59m and 12.56m from the paddle. For each

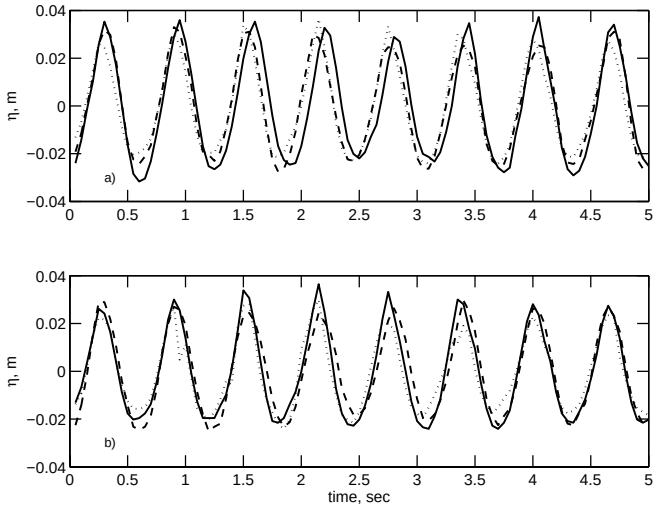

FIGURE 10. Time series of surface elevations η measured at the first wave probe. a) Waves of $U/c = 0$ and $IMF = 1.6$Hz for different IMS: 0.31 (solid line), 0.25 (dashed line), 0.23 (dotted line). b) Waves of $IMS = 0.23$ and $IMF = 1.6$Hz under different wind forcing: $U/c = 0$ (solid line), $U/c = 1.4$ (dashed line), $U/c = 11$ (dotted line). The waves propagate from right to left.

record, IMS was varied in such a way that the waves would consistently break just after one of the wave probes. In this way, the dimensional distance to breaking, wave train properties immediately prior to breaking and detailed properties of the incipient breaker could be measured. Note that this breaker is a result of nonlinear wave evolution, rather than being forced or simulated by means of, for example, coalescing wave packets.

In figures 10 and 11, time series of surface elevations η at the first and the second wave probes are shown. All the waves in these time series are generated with the same Initial Monochromatic Frequency $IMF = 1.6$Hz, but with different initial steepness IMS and wind forcing U/c, as indicated.

Subplot a) of figure 10 corresponds to zero wind forcing. Since the initial steepness of $IMS = 0.31$ (solid line), 0.25 (dashed line) and 0.23 (dotted line) is quite high, modulation is already visible developing at the first probe (figure 10), 4.55m from the wavemaker. At this stage, the modulation is still quite weak, and differences other than those due to the initial wave height are hardly distinguishable.

In subplot b), waves of $IMS = 0.23$ are plotted with no wind forcing (solid line, for cross-reference with the top panel), $U/c = 1.4$ (dashed line) and a very strong wind of $U/c = 11$ (dotted line). The effect of the wind on the profile of the mechanically-generated waves is not noticeable at this first probe, except for the extreme forcing case, where wind-generated ripples are clearly visible in the time series.

The wave profiles look very different at the second probe, 10.53m from the paddle, some 10 wavelengths downstream (figure 11). In all the cases, breaking still has not occurred. Waves in the top three panels evolve without wind forcing, and in the bottom subplot waves are shown strongly forced ($U/c = 11$).

Figure 11a shows initially very steep waves of $IMS = 0.31$. By the time they reach probe 2, they have developed into very strongly modulated groups of 6 waves. Less initially steep waves ($IMS = 0.25$, figure 11b) evolve into more elongated modulated groups of some 7 waves. Even less steep waves ($IMS = 0.23$, figure 11c) evolved into

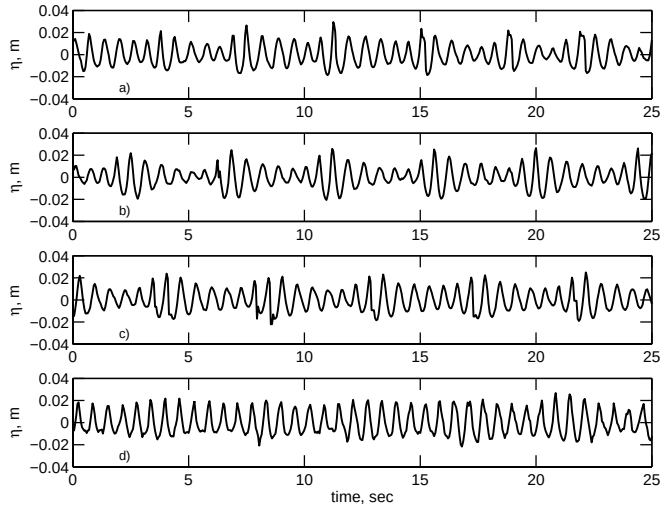

FIGURE 11. Time series of surface elevations η measured at the second wave probe, $IMF = 1.6$Hz. a) $IMS = 0.31, U/c = 0$. b) IMS=0.25, U/c=0. c) IMS=0.23, U/c=0. d) IMS=0.23, U/c=11. The waves propagate from right to left.

weaker modulated groups of approximately 7.5 waves (15 waves in two modulations). Note that no initial modulation was introduced. This interesting observation is, however, not unexpected and is in full qualitative agreement with the discussion in Section 1: i.e. if M_I for the system does not change, a larger initial steepness should lead to fewer waves in the modulation.

The effect that the wind forcing has on BF modulation is demonstrated in figure 11d. Here, we define the modulation depth R to be

$$R = \frac{H_h}{H_l}, \tag{3.1}$$

where H_h and H_l are the heights of the highest and lowest waves in the group. In figure 11c and 11d waves of $IMS = 0.23$ are shown without wind and with wind, respectively. The influence of wind is revealed in the reduction in R from 2.1 without wind, to 1.3 with a wind of $U/c = 11$. As pointed our by our Reviewer, it is the crests' change that appears the main reason for the sharp decrease in R.

It was observed that this change also led to a very significant reduction in the breaking severity (section 3.4 below). The severity (energy loss in a breaking event) is a very important breaking property as, along with the frequency of breaking occurrence (breaking rate), it defines the energy dissipation in a wave field.

3.2. *Measurements of the evolution of nonlinear waves to breaking*

Nonlinear evolution of two-dimensional laboratory waves to breaking will now be investigated in a fashion similar to the numerical study of Section 2. The nonlinear characteristics of interest (i.e. individual wave steepness, skewness and asymmetry), will be obtained by means of zero-crossing selection and analysis of individual waves. In addition to these three characteristics, we will scrutinise the behaviour of the period (frequency) of individual nonlinear waves. This feature was not identified in the dimensionless numerical simulations, but in the laboratory it appears to be quite variable, even in the

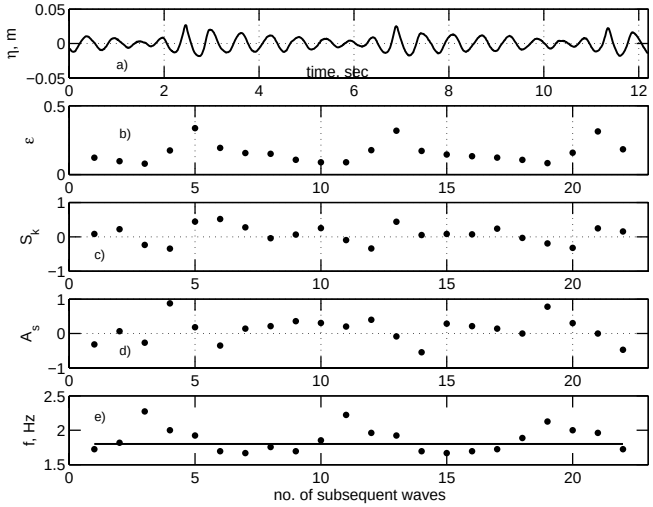

FIGURE 12. Segment of a time series with $IMF = 1.8$Hz, $IMS = 0.30, U/c = 0$. a) Surface elevation η. b) Rear-face steepness ϵ. c) Skewness S_k (rear trough depth is used). d) Asymmetry A_s. e) Frequency. $IMF = 1.8$Hz is shown by the solid line. The waves propagate from right to left.

train of waves of initially uniform frequency. The effect of such local frequency variation is significant for the breaking-onset study since, when wave height growth is accompanied by a synchronous reduction of wave period, this has a combined impact on the local wave steepness.

It should be noted that there is a conceptual change in the frame of reference compared to the numerical model results. In the case of the model, a single wave was followed as it approached the point of breaking. Here, observations are made at a single point as a succession of waves passes. One can approximately move from the fixed frame of reference in the figures of this section to the moving frame by considering the waves shown propagating from right to left, rather than from left to right as in the figures of Section 2.

Figure 12 shows a wave record with $IFM = 1.8$Hz, $IMS = 0.30$ and no wind forcing, measured at the second probe. In figure 12a, the measured water surface elevation η is plotted as a function of time in seconds, and in all the other subplots the dots correspond to the successive waves selected by zero-crossing means. The highest waves in each modulation are incipient breakers as IMS was chosen such that the point of breaking was located immediately after the probe at a distance of 10.73 ± 0.1m from the wavemaker. The apparent consistency of the shape of these near-breakers allows an investigation of characteristic geometric properties of the breaking onset (see section 3.3 below). Here, we should mention that the forward- and rear-face troughs of waves often have different depths. H is always defined in terms of the rear height, and thus the local steepness and skewness are defined as the rear-face steepness and skewness.

Each successive wave passing the wave gauge was analysed to determine its steepness, skewness, asymmetry and frequency, which are shown in the bottom four panels of figure 12. The major features seen in the numerical model are confirmed by the laboratory data. In figure 12b, the steepness $\epsilon = kH/2$ of the 22 individual waves is shown. As expected from the numerical simulations, the incipient breakers are the steepest waves in the train, and the individual steepness oscillates in a periodic fashion. Skewness (fig-

ure 12c) and asymmetry (figure 12d) oscillate with the same period, in phase and in quadrature respectively. At the point of breaking, skewness is positive and maximum (i.e. wave is peaked up) whilst asymmetry is small (i.e. wave is not tilted forward) and keeps decreasing.

It is worth mentioning that oscillations of the skewness and asymmetry obtained in our two-dimensional simulations and experiments are also observed in directional wave fields. In Agnon *et al.* (2005), a methodology was developed to describe fine-scale inhomogeneity of wave-field skewness and asymmetry. Continuous time series of skewness were obtained as a running average of the third moment of surface elevation, and asymmetry as a running average of the third moment of the Hilbert Transform of the surface elevation. It was found that in field conditions wave skewness and asymmetry oscillate at a scale of a few wave periods.

A feature which was not determined from the dimensionless numerical model is that there is also a modulation of the frequency of individual waves (figure 12e). This modulation takes place at the same scale as oscillations of the other nonlinear characteristics. At the point of breaking the frequency increases rapidly, further increasing the steepness and hastening the onset of breaking. Since the time series, rather than space series are measured, the observed shortening of the period can mean that either the waves crest is travelling faster or the wavelength is decreased, or both.

The permanent nature of the patterns in figure 12 highlights a deterministic, rather than random character of the breaking onset in our experiments, driven by the initial nonlinearity of the waves. The combined sudden increase in the wave height and contraction of the wave period prior to breaking is a significant feature of the breaking onset. If, as suggested in Section 2, loss of water-surface stability rather than anything else defines the breaking, then this feature certainly contributes to reaching the critical local steepness. Once detected, for example by wavelet techniques, it may signify the imminent onset of breaking.

This change of frequency prior to breaking is further illustrated in figure 13a where the spectrum of the time series of figure 12 is plotted. If the wave of $IMF = 1.8$Hz simply evolved into a steep Stokes wave, a 1.8Hz peak of the spectrum would bring about 1st, 2nd and 3rd harmonics indicated by the vertical solid lines. In figure 13a, however, the harmonics, as well as the peak itself are now defined by the incipient breaker. The harmonics are located at double, triple and quadruple frequencies of this breaker whose frequency is about 2Hz (vertical dashed lines).

Therefore, immediately prior to breaking, a frequency upshift of the spectral energy occurs in the laboratory two-dimensional situation. This feature has also been previously observed in the field for breaking directional waves (Liu & Babanin 2004). As with the field observation of skewness/asymmetry oscillations mentioned above, this is indirect, but encouraging corroboration that the present two-dimensional study may have relevance for real three-dimensional waves.

In addition, independent observations report a frequency downshift due to breaking (e.g. Tulin & Waseda 1999; Meza *et al.* 2000). Wave series immediately before and after the breaking are compared in figure 14. In this figure, the solid line shows the waves of $IMF = 1.8$Hz, $IMS = 0.30, U/c = 0$ at the second probe (10.53m from the wavemaker), as in figure 12, and dashed line – at the third probe (11.59m from the paddle). Breaking of the three incipient breakers seen at probe 2 happened (started and finished) between the two probes. The wave which is seen following the incipient breaker at the second probe also broke between the two probes. This consistent double-breaking, with a small time delay, is again in agreement with field observations (e.g. Donelan *et al.* 1972). These breaking processes happened in a period of 1.2s, the time required by the 1.8Hz waves

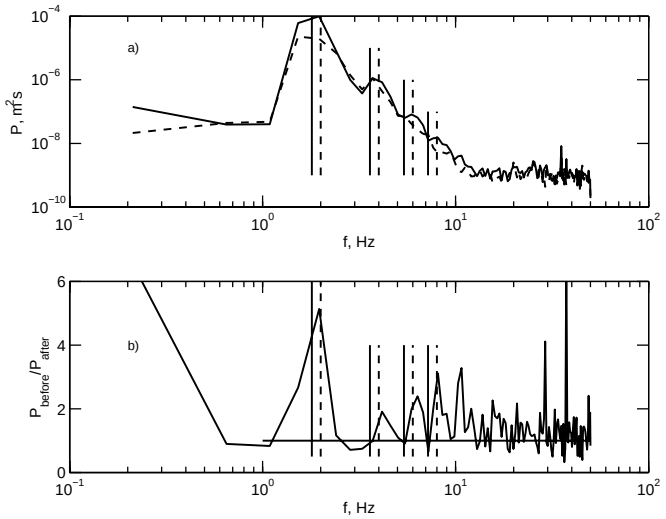

FIGURE 13. a) Spectra P of the time series of $IMF = 1.8$Hz, $IMS = 0.30, U/c = 0$. Solid line corresponds to the pre-breaking spectrum measured at the second probe (see time series in figures 12). Dashed line is post-breaking spectrum measured at the third probe (time series in figure 14). Multiples of IMF are shown with solid vertical lines. Multiples of the incipient-breaker 2Hz frequency are shown with dashed vertical lines. b) Ratio of the pre-breaking and post-breaking spectra. Solid horisontal line signifies ratio of 1, vertical lines have the same meaning as in the top panel.

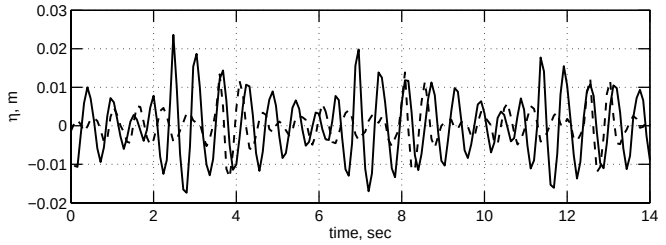

FIGURE 14. The influence of breaking on the time series. A segment of the surface elevation time series with $IMF = 1.8$Hz, $IMS = 0.30, U/c = 0$. Solid line - surface elevations at the second probe prior to breaking. Dashed line - same waves 1.2s later at the third probe. The waves propagate from right to left.

to travel the distance between the probes. Therefore, the record made at the third probe is time-shifted by 1.2s in an attempt to superimpose what should have been the same waves, if the breaking did not take place.

Now that breaking has occurred, the correlation between the two time series is poor. The incipient breaker and wave following it practically disappeared, as well as the entire modulation. The only waves which can still be tracked are the second and the third wave after the incipient breaker at probe 2. The number of waves in the segment has also changed. Between the three incipient breakers at probe 2 one can count 17 waves, at probe 3 this number is closer to 16, i.e. frequency downshifting has occurred.

This frequency downshift is analysed in spectral terms in figure 13a where, along with the spectrum at probe 2, the probe-3 spectrum is also plotted. The downshift from the

2Hz peak of the incipient breaker is very significant, and is also noticeable with respect to $IMF = 1.8$Hz which was the peak frequency in the wave field before the point of breaking onset. As indicated above, this feature has been observed before (e.g. Tulin & Waseda 1999). In our experiments, the downshift occurs on a time scale of tens of wave periods. This is is much faster than the scale of thousands of wave periods for the four-wave resonant nonlinear interactions are usually attributed with the downshifting.

Apart from the frequency downshift, a significant loss of wave energy is observed between the two spectra shown in figure 13a. In figure 13b, the ratio of the pre-breaking spectrum to the post-breaking spectrum is plotted. In the range of relevant frequencies up to 11Hz, the average ratio is 1.8, which translates into a loss of 45% of the energy. It is most instructive to analyse where this loss comes from.

In both absolute and relative terms, most of the loss came from the peak which was reduced by a factor of 5. With the exception of the second harmonic (shifted to 3.6Hz), the other harmonics have almost completely disappeared. For frequencies above the spectral peak, the average ratio is approximately 1.7.

This result contradicts observations by Meza *et al.* (2000) who studied the dissipation of energy of laboratory two-dimensional waves with a narrow spectrum. They found that the energy is lost almost entirely from the higher frequencies whereas the spectral peak remained unchanged after breaking. In Meza *et al.* (2000), as in many other laboratory investigations, breaking was simulated by means of coalescing wave packets - i.e. dispersive linear waves were generated by the wave paddle such that, due to their phase speed differences, superposition occurred at the point of the measurements. The superposition formed a high wave which broke. The limiting steepness of such waves $ak = 0.44$ (Brown & Jensen 2001) is the same as the steepness of the incipient breaker measured in this study (section 3.3), but the physics of this breaking appears to be quite different to the physics of our experiment. In the present experiment, the breaking results from nonlinear evolution of non-dispersive waves. Thus, issues of the wave breaking and the wave energy dissipation need to be separated as will be further discussed in Section 4 below.

Under field conditions, Young & Babanin (2006) observed that when the dominant waves break they lose some 30% of their energy and a similar amount of energy is also lost proportionally across the spectrum, the so-called cumulative effect. By obvious analogy, such observation again suggests the nonlinear evolution mechanism, rather than wave superposition, as a likely cause of wave breaking in the field. The modulational instability may have limitations in directional fields (see discussion in Section 4), and it is clear that at least some part of the cumulative effect in the field spectral environment is due to induced breaking (Manasseh *et al.* 2006) and residual turbulent viscosity (Babanin & Young 2005), i.e. reasons other than removal of bound energy observed in figure 13 above. It is obvious, however, that the modulational-instability mechanism is more consistent with field results than the linear-superposition breaking, which does not provide a satisfactory explanation of the observed field features.

3.3. *Measurements of the breaking onset*

While the properties of waves breaking due to focusing coalescing packets have been previously described in great detail (e.g. Rapp & Melville 1990), physical characteristics of breaking resulted from the nonlinear wave evolution have rarely been measured. This is despite the fact that a great number of geometric, kinematic and dynamic criteria have been proposed for such breaking over the years (e.g. Longuet-Higgins 1969; Holthuijsen & Herbers 1986; Caulliez 2002).

As the location of the breaker can be controlled by varying the IMS at the wavemaker, the waves were made to break immediately after a wave probe and thus the properties

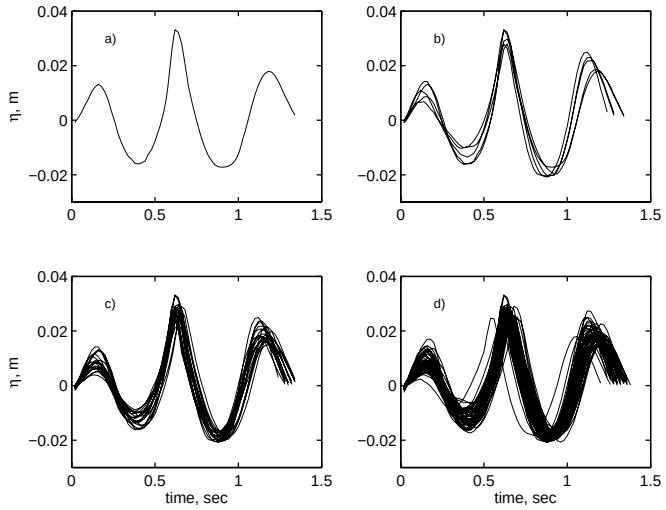

FIGURE 15. IMF=1.8Hz, IMS = 0.30, U/c=0. a) The steepest incipient breaker. b) Five steepest incipient breakers. c) Twenty steepest incipient breakers. d) Fifty steepest incipient breakers. The waves propagate right to left.

of incipient breakers could be directly measured. Figure 15 shows one, five, twenty and fifty steepest breakers in consecutive panels. No normalisation has been applied and the waves are plotted as they appear in physical space, from the front zero-crossing of the wave preceding the breaking to the rear zero-crossing of the following wave. Typical features of waves just prior to breaking can now be analysed. The nearly-breaking wave is the highest and most skewed, and is only slightly asymmetric. The two waves immediately preceding and following the breaker are asymmetric: the preceding wave is tilted backward (positive asymmetry) and the following wave is tilted forward (negative asymmetry). The preceding wave is smaller than the following wave, and, at least in these observations, the preceding trough is shallower.

Quantitative characteristics of these waves are further analysed in figures 16-17. Figure 16 shows a comprehensive set of statistics of the properties of the 20 highest incipient breakers and their relationship with the preceding and following wave. Figure 16a is a plot of skewness versus steepness. Values of limiting local steepness, the property which was revealed by the model as the likely indicator of breaking, is in the range of $2\epsilon \approx 0.8$. For a real wave, even if two-dimensional, such steepness is extremely high. Noting that near the crest the wave is even steeper, it is not surprising that the wave is on the point of collapse.

The skewness of the 20 highest waves in subplot (a) scatter from almost 0 to almost 1. As indicated in the simulations in Section 2, we would expect the skewness to also have a limiting value. Clearly, however, such a limit is not a very robust breaking characteristic. Also in the top row of subplots, asymmetry is scattered from $A_s = -0.33$ to $A_s = 0.75$ (b), with a possible dependence of S_k on A_s in panel (d).

A robust property of the breaking, in panel (c), is the wave frequency. The scatter of this property is small, with all the values falling into a range from $f = 2$ to 2.08 Hz (from 1.11 to 1.16 IMF). Thus, the wave clearly reduces in length prior to collapse. We should mention that the measured steepness $\epsilon = kH/2$ is the physical rear-face steepness, and therefore the effect of period contraction has already been accounted for.

In the second row of plots, the skewness of the wave following the incipient breaker

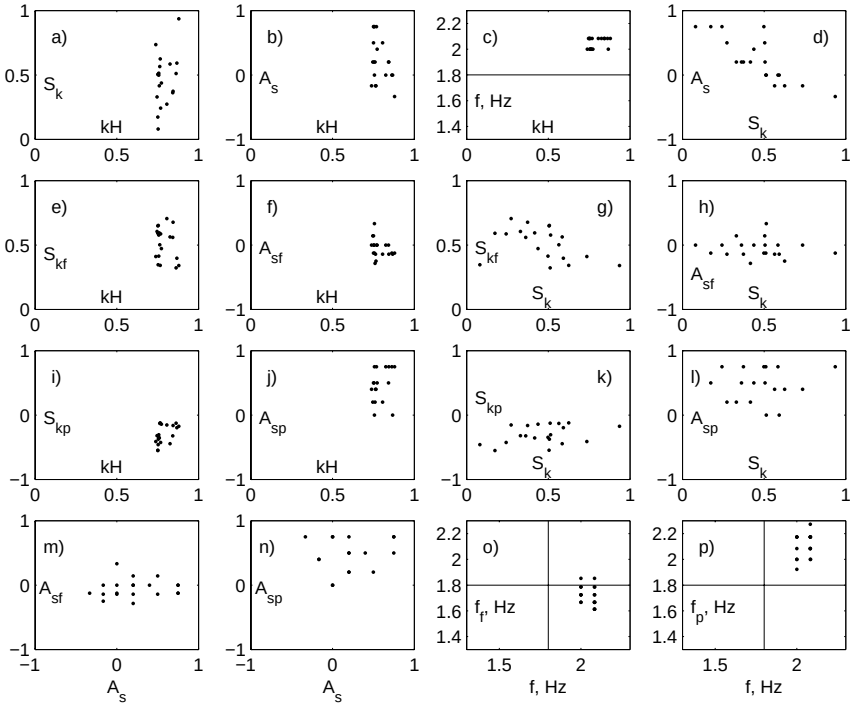

FIGURE 16. Laboratory statistics for the incipient breaker (20 steepest breakers). $IMF = 1.8$Hz, $IMS = 0.30, U/c = 0$. In the figure, S_{kf} and S_{kp} correspond to the skewness of the following wave and preceding wave respectively, A_{sf} and A_{sp} to the asymmetry of the following wave and preceding wave respectively, f_f and f_p to the frequency of the following wave and preceding wave respectively. (a) Skewness versus steepness. (b) Asymmetry versus steepness. (c) Frequency (inverse period) versus steepness. $IMF = 1.8$Hz is shown with solid line. (d) Asymmetry versus skewness. (e) S_{kf} versus steepness of the breaker. (f) A_{sf} versus steepness of the breaker. (g) S_{kf} versus skewness of the breaker. (h) A_{sf} versus skewness of the breaker. (i) S_{kp} versus steepness of the breaker. (j) A_{sp} versus steepness of the breaker. (k) S_{kp} versus skewness of the breaker. (l) A_{sp} versus skewness of the breaker. (m) A_{sf} versus asymmetry of the breaker. (n) A_{sp} versus asymmetry of the breaker. (o) f_f versus frequency of the breaker. $IMF = 1.8$Hz is shown with solid lines. (p) f_p versus frequency of the breaker. $IMF = 1.8$Hz is shown with solid lines.

(e) and its asymmetry (f) are much less scattered than the skewness and asymmetry of the breaker itself: $S_{kf} = 0.32$ to 0.70, $A_{sf} = -0.29$ to -0.33. We have already discussed the double-breaking in section 3.2, which means that this following wave will break soon after the incipient breaker. Thus, its physical shape is not random and should exhibit some characteristic properties leading to breaking. The skewness and asymmetry of the following wave, however, do not correlate with the skewness and asymmetry of the breaker (g, h, m).

In the third row, the skewness of the wave preceding the breaker is even less scattered: $S_{kp} = -0.55$ to $+0.12$ (i). Remarkably, it is essentially negative, i.e. rear trough of the preceding wave is always deeper than its crest. The asymmetry $A_{sp} = 0$ to 1.33 is never negative (a couple of large $A_{sp} = 1.33$ values are offscale in panel (j) and not shown), that is this wave is tilted backward. There is no correlation of skewness and asymmetry of this preceding wave with those of the near-breaker (k, l, n). The fact that the three waves, surrounding the breaking event, obviously exhibit some quasi-universal form, but that variations of their shape are not correlated with each other, means that these shape

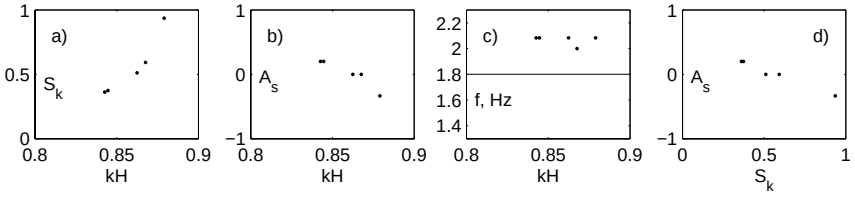

FIGURE 17. As the top four subplots in figure 16, for 5 steepest breakers

distortions are random. Therefore, it is not the mean characteristics of the observed shapes, but rather their limiting values which should produce asymptotic universal form parameters. These will be investigated for the highest breakers in figure 17.

The last two subplots (o, p) show the local frequency of the following f_f and preceding f_p waves versus the frequency of the breaker f_b. $IMF = 1.8$Hz is shown with two solid lines. The local frequency was found to be a robust characteristic for the incipient breaker above, and we can expect a reasonable correlation of these properties. Although f_f and f_p are more scattered than f_b the correlation is present. In the last panel, all the data points are in the second quadrant and thus the preceding wave is decreasing in length along with the incipient breaker. In panel (o), the points are on average in the fourth quadrant. Therefore, while the incipient breaker is decreasing in length, the following wave is actually longer than its initial value defined by $IMF = 0.18$Hz. Since we know that double-breaking will occur, i.e. this following wave will break shortly after the current breaker, then it should now be rapidly shrinking. Thus, some very active physics must be involved in the short-time scale evolution of this set of very nonlinear waves.

Figure 17 shows asymptotic, rather than statistical properties of the incipient breaker. In this figure, the characteristics of the 5 steepest waves are plotted. As discussed above, transition to breaking happens very rapidly, and breaking onset and its location may be somewhat modulated due to, for example, uneven number of waves in the nonlinear oscillations. Thus, we would expect that it is the highest waves measured that would be closest to the ultimate limiting characteristics of the incipient breaker.

For the steepest five waves shown in figure 17, the asymptotic dependence of skewness on steepness is very clear (a). Note that they indeed approach some limit and we had to zoom in to see the variation. Therefore the scale of this subplot is different to that of figure 16. For the 20 steepest incipient breakers, skewness was broadly scattered, now that onset is close, it asymptotes to a value of 1, i.e. crest of the wave which is just about to start breaking is twice as high as its trough (2.14).

The steepness appears to approach an asymptotic limit of $\epsilon = kH/2 \approx 0.44$ which apparently represents an absolute steepness limit (Babanin *et al.* 2007a). We should point out that this limit is remarkably close to the theoretical steady limiting steepness of $ak = 0.443$, i.e. the Stokes limit $H/\lambda = 1/7$ where $\lambda = 2\pi/k$ is the wavelength. Such an observation is very important because it signifies that the waves break once they achieve this well-established state, beyond which the water surface cannot retain its stability. This limit was established as a stationary solution, and further theoretical investigations are needed into the limiting state of non-stationary waves. From this experiment, however, it is obvious that a wave of such extreme steepness is unstable and will start collapsing. Thus the limiting steepness, rather than anything else, will trigger the breaking. We can postulate that the other geometric, kinematic and dynamic criteria of breaking, explored in the literature, are indicative of a wave approaching this state, but are not a reason or a cause for the breaking. As this limit is approached, the skewness increases very rapidly

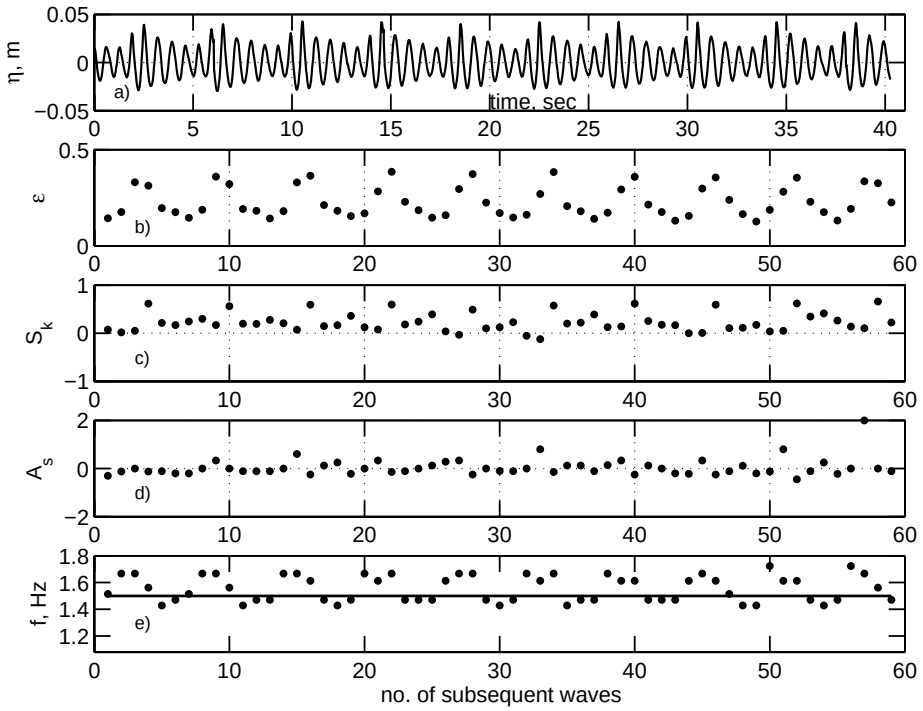

FIGURE 18. As in figure 12, with wind forcing. A segment of the time series with $IMF = 1.5$Hz, $IMS = 0.30, U/c = 3.9$. a) Surface elevation η. b) Rare-face steepness ϵ. c) Skewness S_k (rare trough depth is used). d) Asymmetry A_s. e). Frequency (inverse period). $IMF = 1.5$Hz is shown with solid line. The waves propagate from right to left.

(a) and the asymmetry starts to decrease and becomes negative (subplots (b) and (d)), i.e. the wave starts tilting forward at the point of breaking.

3.4. *Laboratory investigation of the influence of wind forcing*

Following the same approach as in the numerical simulations in Section 2, we now investigate the influence of wind on the nonlinear wave evolution and breaking onset. The wind has been shown to play multiple roles in the wave evolution to breaking. At larger scales, the wind generates and pumps energy into the waves, increasing their steepness and thus leads to more frequent breaking. At moderate wind conditions, doubling the wind speed resulted in the breaking occurring four times faster (e.g. figure 4). Instantaneously, at the point of breaking onset, the capacity of the wind to push the wave over and thus affect the onset is small, even if the wind is very strong and a wave is very steep (figures 8-9). At medium scales, however, the wind changes the modulational depth R (3.1) of already existing waves (figure 11), which changes appear to be linked with alterations of the breaking severity.

Figure 18 is similar to figure 12, but moderately strong wind forcing of $U/c = 3.9$ is now applied to the mechanically generated waves. Note that $IMF = 1.5$Hz is different from $IMF = 1.8$Hz in figure 12. This is done in order to have incipient breakers, as before, at the probe 2 where data is recorded. With the wind superimposed, the waves of $IMF = 1.8$Hz, $IMS = 0.30$ would break before this probe (see discussion in sections 2.2 and 4, and figures 6 and 24).

In figure 12, $R = 4$ whereas in the current figure 18 $R = 2.9$, i.e. the difference in the

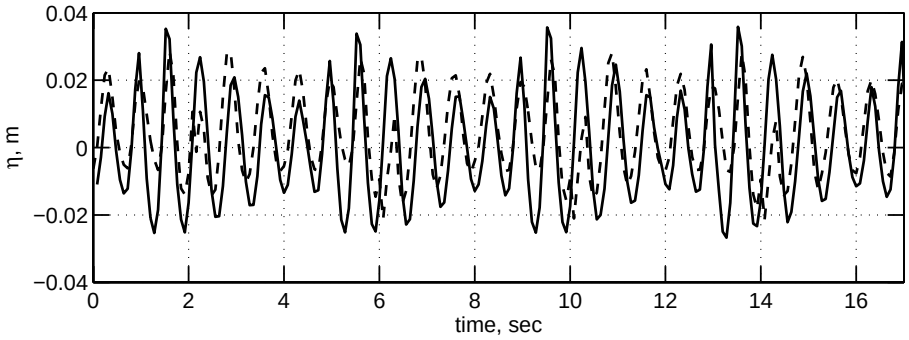

FIGURE 19. As in figure 14, with wind forcing. A segment of the time series with $IMF = 1.5$Hz, $IMS = 0.30, U/c = 3.9$. Solid line - surface elevations at the second probe prior to breaking. Dashed line - same waves 1.04s later at the third probe. The waves propagate from right to left.

modulation depth is 1.4 times. Thus, we observe the expected feature of smearing of the modulation by the wind. This smearing is reflected in all the other nonlinear properties shown in the figure. The steepness (b), skewness (c) and asymmetry (d) are intentionally plotted at the same scale as those in figure 12 even though their range of oscillations is now noticeably reduced. Because of the IMF change, the scale of the frequency plot (e) could not be left the same, but scale limits were kept proportional to those in figure 12. Reduction of the local frequency oscillations, moderated by the wind, is also apparent.

Influence of the smearing on the wave breaking is demonstrated in figure 19. This figure is analogous to figure 14 except the wind forcing is now superimposed and $IMF = 1.5$Hz is different as explained above. The wave time series are compared immediately before and after breaking. The solid line shows the waves of $IMF = 1.5$Hz, $IMS = 0.30, U/c = 3.9$ at the second probe (10.53m from the maker) and the dashed line at the third probe (11.59m from the paddle). Breaking of the four incipient breakers seen at probe 2 occurred (started and finished) between the two probes. The breaking was very gentle when visually observed. The wave following this gentle incipient breaker now does not break, i.e. the wind cancelled the double-breaking effect. With $IMF = 1.5$Hz, the time necessary to travel the distance between the two probes is estimates as 1.04s and therefore the record made on the third probe is shifted back by 1.04s in order to superpose what should be the same waves if the breaking did not take place.

Since gentle breaking did occur, matching the two series is not exact. In figure 14, the incipient breaker and the wave following it practically disappeared, as well as the entire modulation. Here they are all present and each wave in the modulation can be tracked at the third probe. In contrast to figure 14, after breaking the number of the waves did not change and no downshifting is visible. As seen in the figure, the breaking resulted in truncation of the crest of the breaker and smoothing of the modulation. It should be pointed out that the individual waves and the group propagate with different speeds which fact also accounts for some differences observed.

The major features of the breaking onset in the presence of wind forcing are shown in figures 20, 21 and 22. Visually, the breakers in figure 20 did not qualitatively change compared to those in figure 15 with no wind. Quantitative properties, however, were altered by the wind.

In figure 21, analogous to the no-wind figure 16, the statistics of a comprehensive set of properties for the 20 highest incipient breakers and their links to the preceding and

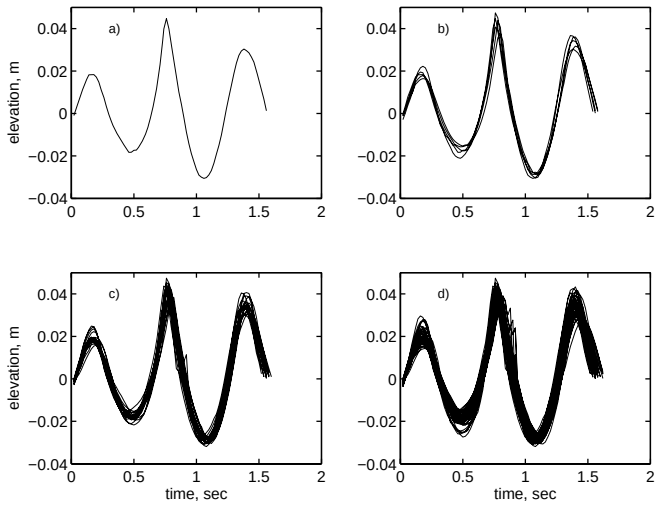

FIGURE 20. As in figure 15, with wind forcing. $IMF = 1.5$Hz, $IMS = 0.30, U/c = 3.9$. a) The steepest incipient breaker. b) Five steepest incipient breakers. c) Twenty steepest incipient breakers. d) Fifty steepest incipient breakers. The waves propagate right to left.

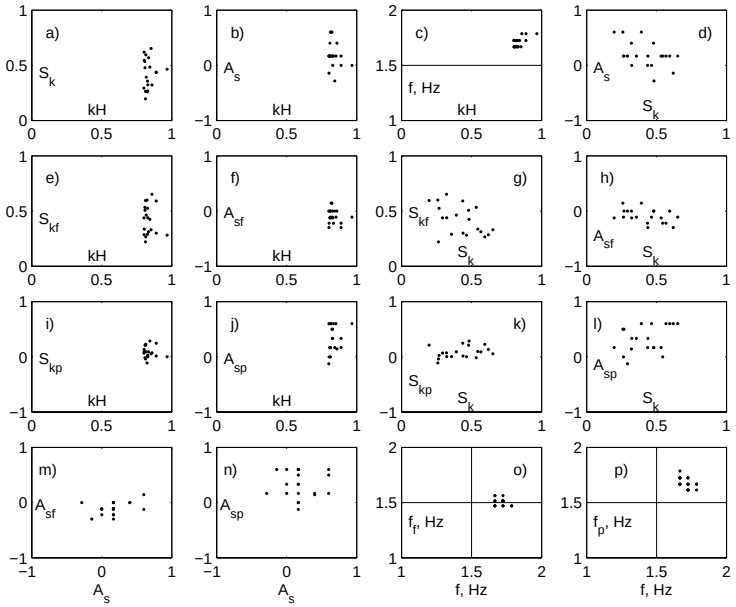

FIGURE 21. As in figure 16, with wind forcing. $IMF = 1.5$Hz, $IMS = 0.30, U/c = 3.9$. Laboratory statistics for 20 steepest incipient breakers.

following wave are shown. For the 20 waves approaching breaking, the wind influence generally brought more order to their shapes, as the scatter of almost all the properties is reduced and the marginal dependences became clearer. Qualitatively, the wind changed the shape of the preceding wave which is now not skewed negatively on average (i) and increased the steepness of the following wave from $\epsilon = 0.19$ to $\epsilon = 0.27$ on average (not shown).

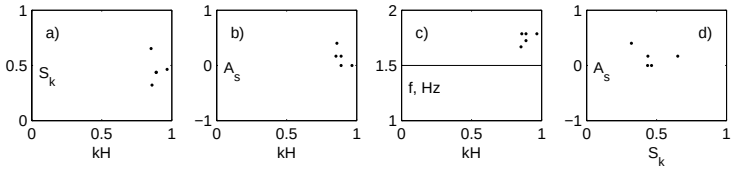

FIGURE 22. As the top four subplots in figure 17, with wind forcing. $IMF = 1.5$Hz, $IMS = 0.30, U/c = 3.9$. Laboratory statistics for 5 steepest incipient breakers.

With regard to the asymptotic shape of the breaker, the wind in figure 22 has a scattering rather than stabilising influence. In this figure, analogous to figure 17, characteristics of the 5 steepest waves are plotted in the presence of wind. Apparently, at these very last pre-breaking stages, the wind is capable of modifying the wave, which is about to lose its stability, and to somewhat randomise its characteristics.

In subplot (a), the limiting skewness is plotted versus limiting steepness. Skewness no longer approaches 1, but steepness extends beyond the $2\epsilon = 0.88$ limit and reaches $2\epsilon = 0.97$. The asymmetry is no longer negative, that is, the breakers do not tilt forward (b). Frequency remains a robust property and stays in almost the same range of $f_b = 1.11$ to $1.19IMF$ (c).

Therefore, whilst the breaking is mainly a hydrodynamic process, wind, if present, does influence the incipient breaking. As was noticed in the numerical simulations, this influence is small, but it is noticeable and diverse – from the shape-stabilising effect when approaching breaking onset to the shape-randomising effect at the point of breaking.

4. Discussion and Conclusions

In the numerical simulations of Section 2, figure 6 was declared the main result because it allowed to predict distance to breaking in dimensionless terms: number of wavelengths to breaking $N = x_{break}/\lambda$ as a function of wave steepness and wind forcing, where x_{break} is the dimensional distance. Examination of its laboratory analogue was moved to this Section as its appicability to field conditions will also be discussed.

The laboratory dependence of the distance-to-breaking on IMS was obtained and parameterised in Babanin *et al.* (2007a). Respective figure of Babanin *et al.* (2007a) is reproduced with modifications as figure 23a here. Number N is plotted versus IMS for three different initial frequencies of $IMF = 1.6$Hz (circles), $IMF = 1.8$Hz (crosses) and $IMF = 2.0$Hz (pluses). All the measurements shown are conducted without wind.

In accordance with the numerical simulations, for each wavelength an increase of its initial steepness resulted in the breaking occuring closer to wavemaker. In dimensionless terms, this dependence was parameterised as follows:

$$N = -11 \cdot atanh(5.5(\epsilon - 0.26)) + 23 \text{ for } 0.08 \leqslant \epsilon \leqslant 0.44. \tag{4.1}$$

Consistent, with the model results, the formula imposes two threshold values of IMS. For $\epsilon > 0.44$, the wave breaks immediately (compared to $\epsilon = 0.3$ for the model) and if $\epsilon < 0.08$ the wave, in the absence of wind forcing, will never break (compared to $\epsilon = 0.1$ for the model).

In the figure, two points (squares) are shown which were derived from figures 1 and 2 of Melville (1982) for comparison. The two measurements were conducted by Melville (1982) for initially uniform wave trains, their initial steepness and approximate dimensionless distance to breaking is known. Although recorded independently under different

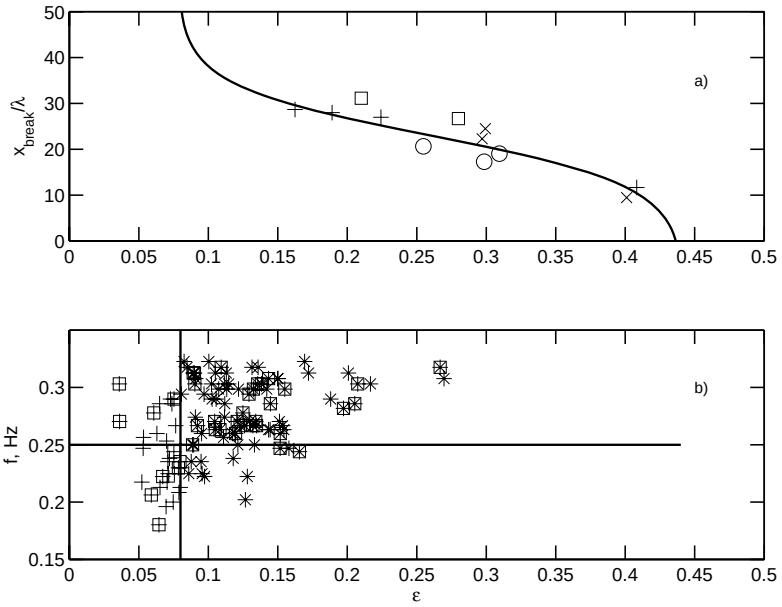

FIGURE 23. a) ASIST laboratory data. Number N of wavelengths to breaking versus IMS. No wind forcing. o - $IMF = 1.6$Hz; x - $IMF = 1.8$Hz; + - $IMF = 2.0$Hz. The parameterisation (4.1) is shown with solid line. Squares are data points derived from Melville (1982). b) Black Sea. Properties of individual waves in the range of frequencies $f = f_p \pm 0.3f_p$ of a Black Sea record with $f_p = 0.25$Hz. Frequency (inverse period) f versus steepness ϵ. + - all waves, * - those waves with $\epsilon > 0.08$, squared - those waves exhibiting whitecapping. Solid lines show peak frequency $f_p = 0.25$Hz (horisontal) and the breaking threshold $\epsilon = 0.08$ (vertical).

conditions and with a different purpose, these points agree very well with the above parameterisation and provide an additional support to our results.

Comprehensive wind-forcing picture similar to the numerical result in figure 6 could not be obtained in ASIST where available range of distances and wavelengths was limited by the tank dimensions. Besides, as pointed out by our Reviewer, presence of a sustained wind in the tank may cause a significant shear layer and vorticity field in the water. The latter can lead to steeper steady free surfaces and thus make direct quantitative comparisons problematic. Qualitatively, however, the laboratory results are in full accord with numerical simulations. In figure 24, number N is plotted versus wind-forcing parameter U/c for four different IMFs: $IMF = 1.5$Hz (circles), $IMF = 1.55$Hz (crosses), $IMF = 1.6$Hz (pluses) and $IMF = 1.7$Hz (asterisks). At each IMF, initial steepness IMS was kept constant, and therefore the apparent trend of reduction of distance-to-breaking is due to wind only.

Before summarising conclusions of the paper, we would like to discuss possibility of application of its results to waves observed in the field. A number of features of nonlinear wave behaviour leading to the breaking, which were revealed both in our 2D simulations/measurements and in known field observations have been mentioned above. Such is the double-breaking found in our laboratory experiments and observed in the field by Donelan *et al.* (1972). Such are upshifting of spectral energy (figures 13, 14) observed in Liu & Babanin (2004), oscillations of the skewness/asymmetry (figures 4, 12) – in Agnon *et al.* (2005), cumulative effect (figure 13) – in Young & Babanin (2006). Gemmrich & Farmer (2004) analysed velocity field under the passing breaker and found upshifting

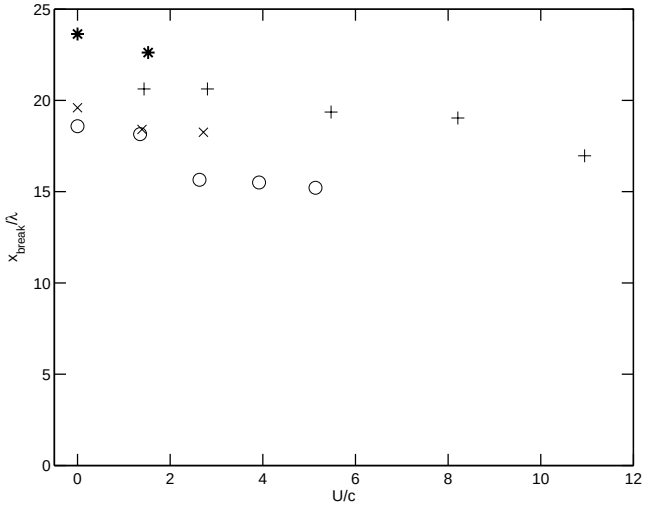

FIGURE 24. Number N of wavelengths to the breaking versus wind forcing U/c. o - $IMF = 1.5$Hz; x - $IMF = 1.55$Hz; + - $IMF = 1.6$Hz; * - $IMF = 1.7$Hz.

of wave energy followed by downshifting (their figure 12), which is qualitatively similar to the upshifting–downshifting observed in this paper (figures 13, 14). Similarly, conclusion of Melville & Matusov (2002) about breaking waves propagating at some 80% of the characteristic linear phase speed can be interpreted as an indirect support of the pre-breaking wave shrinkage. The fact that doubling the wind input brings about wave breaking four times as fast (section 2.2, figure 4) is consistent with field experiments on wind input (Donelan *et al.* 2006). Although all these evidences are indirect, the very quantity of them indicates some quality.

What is against direct extrapolation of outcomes of the present paper into field conditions is known experimental and theoretical results on limitations which BF mechanism has in broad-band, and particularly in three-dimensional fields (e.g. Brown & Jensen 2001; Onorato *et al.* 2002, 2008; Waseda *et al.* 2008). We concluded that modulational instability is the driving force behind nonlinear evolution of our waves to breaking, and since our study was initially-monochromatic and two-dimensional, and field waves are spectral and directional, this issue has to be addressed before applying our results to such waves.

Brown & Jensen (2001) studied the focusing of unidirectional waves and found that BF instability is impaired in focusing (i.e. spectral) wave trains. Such study needs to be extended into spectra typical of field waves and examined further. There is a reasonable expecation, however, that the modulational mechanism may work for reasonably steep waves with a narrow spectrum (e.g. Waseda *et al.* 2008). For unidirectional spectral waves, Alber (1978) derived a requirement which can be expressed as

$$M_I > 1, \tag{4.2}$$

and this condition can be satisfied for spectra of young wind waves (e.g. Onorato *et al.* 2001).

There is no analogue of M_I and condition (4.2) available for three-dimensional characteristics of the modulational instability mechanism. In Onorato *et al.* (2002), directional effects were investigated and quantitative criterion β was obtained in terms of width of

directional spectrum $D(\theta)$ where θ is angle:

$$D(\theta) = cos^2(\frac{\pi}{2\beta}\theta) \tag{4.3}$$

– i.e. if the directional width is greater than $\beta = 15$, then the modulational instabiltiy appears to be suppressed. There was a typing error in Onorato *et al.* (2002), and value of β has to be actually multiplied by $\pi/180$, that is the criterion is $\beta \approx 0.26$ (Onorato, 2007, personal communication). Since the Onorato *et al.* (2002) model is weakly nonlinear rather than fully nonlinear, the criterion should only be regarded as an approximation, but we will use it as a reference point here.

To compare width of the (4.3) spectrum with observations, integral value A was estimated:

$$A^{-1} = \int_{-\beta}^{\beta} D(\theta) d\theta \tag{4.4}$$

which was used in the field study of Babanin & Soloviev (1998a) to measure directional distributions (the higher is A, the narrower is the spectrum). For $\beta = 0.26$, $A = 3.8$ which is well above the experimentally observed values. It should be mentioned that this theoretical value is in excellent agreement with the laboratory experiment of Waseda *et al.* (2008) who concluded that the critical directional spread is $A \approx 4$.

Modulational instability, however, may still be found applicable, at least for the dominant waves if they are steep enough. It is not unreasonable to expect a directional condition analogous to (4.2) being relevant. Parameter A (4.4) can be used for this purpose as it has the proper physical meaning of the inverse relative width of the directional spectrum whose peak is normalised to be 1.

At the spectral peak, a relative steepness (as the wave spectrum develops) is defined by $\sqrt{\gamma}$ where γ is the peak enhancement of the JONSWAP spectrum. That is, for the peak, we can define a directional analogue of M_I as

$$M_{Id} = A\sqrt{\gamma}. \tag{4.5}$$

Now, it is informative to look at how this Index evolves over the wave development. From (Eq.19) of Babanin & Soloviev (1998a), at the spectral peak

$$A = 1.12(\frac{U_{10}}{c_p})^{-0.50} + (2\pi)^{-1}, \tag{4.6}$$

and from (Eq.44) of Babanin & Soloviev (1998b)

$$\gamma = \frac{7.6}{2\pi}\frac{U_{10}}{c_p}, \tag{4.7}$$

that is

$$\sqrt{\gamma} = 1.10(\frac{U_{10}}{c_p})^{0.50}. \tag{4.8}$$

Therefore,

$$M_{Id} = 1.23 + \frac{1}{2\pi}(\frac{U_{10}}{c_p})^{0.50} \tag{4.9}$$

is a weak function of the wind forcing, and its value at the spectral peak varies from 1.40 to 1.79 for $\frac{U_{10}}{c_p}$ in the range from 0.89 to 10 where $\frac{U_{10}}{c_p} = 0.89$ signifies full developemnt (Pierson-Moscowitz limit).

Now, if the M_{Id} assumption is valid and the critical value for this Index is in the range of $M_{Id} = 1.4 - 1.8$, the 'focusing' effect of directionality can be overcome by a stronger

nonlinearity if waves grow steeper. It is worth noting here that the directional spectra broaden towards frequencies above the peak (e.g. Babanin & Soloviev 1998a). This means that, even if applicable at the peak, the directional modulational instability may not be working at higher frequencies and some other causes of breaking and dissipation will have to be found in that spectral band. In this regard, two-phase behaviour of the breaking has indeed been observed in field experiments of Babanin & Young (2005); Manasseh *et al.* (2006) - i.e. the direct dependence of breaking on spectral density at the peak and an induced breaking/dissipation at higher frequencies.

In any case, the issue of modulational instability in real spectral directional fields cannot be solved now, but with caution we will try to apply our results to the field data. Another problem, of the technical kind, still prevents direct comparisons of breaking rates obtained by means of (4.1) and field observations. Relationship (4.1) predicts the probability of incipient breaking, whereas in the field it is impossible to directly measure whether a wave is an incipient breaker or not. At best, we can detect quantities which result from the breaking process, that is we count waves already breaking. Common measures of this type include the acoustic signature of breaking waves, void fraction or surface whitecap coverage. However, a breaking wave emits sound and forms whitecaps over a substantial part of its period whereas the incipient breaking is an instantaneous state, and therefore the probability of encountering such sound or whitecaps is significantly higher than the probability of breaking onset (Liu & Babanin 2004).

Qualitative comparisons of the laboratory and field breaking-probability dependences were done in Babanin *et al.* (2007a) and featured well. Here, in figure 23 (bottom) we plot frequency (inverse period) of individual dominant waves (from frequency range of $f = f_p \pm 0.3f_p$) versus steepness of these individual waves. This is done for a Black Sea record with $f_p = 0.25$Hz used by Babanin *et al.* (2001) to obtain field breaking rates in the same frequency band. If there was no shrinking of the wavelength prior to breaking, as described in this paper, at each steepness the distribution of the frequencies around $f_p = 0.25$Hz would be approximately even. It is so for waves of $\epsilon <\approx 0.12$. For steeper waves, and some of these detected deep-water wind-generated three-dimensional waves have an enormous by field standards steepness up to $\epsilon = 0.27$, the distribution is clearly biased towards higher frequencies. Waves with $\epsilon > 0.17$ are all shorter than those of the peak frequency $f_p = 0.25$Hz, and the higher is the individual steepness, the higher is the individual frequency. Since on average the highest waves are observed at the peak frequency, and the peak is very sharp, the only plausible explanation for this observation is that these abnormally steep, but rare waves are those in transition towards or just after the incipient breaking. As deep-water waves below the peak do not break, and if the near-breakers shorten, distribution of the incipient breakers has to be characterised by higher-than-peak frequencies at abnormally high steepnesses as it is. Thus, the very existence of such abnormally high and shrunk waves indicates that the modulational instability mechanism is most likely still active in these field conditions.

It is very informative to see in this plot which waves are detected as breaking by observing whitecaps. Such waves are indicated by squares. Liu & Babanin (2004) classified phases of the wave breaking process into incipient, developing, subsiding and residual stages. At the incipient phase, waves are at their steepest and the surface has already lost its stability, but there are no whitecaps formed. Whitecaps are observed at developing and subsiding stages. The latter phase is characterised by very broken shape of waves and their steepness measured as ratio of wave height to length may be well below the field average. The last, residual stage was introduced formally following Rapp & Melville (1990) as such phase of breaking progress when the whitecap is already left behind, but the turbulent front is still moving downstream.

In figure 23 (bottom), vertical solid line identifies the threshold of $\epsilon = 0.08$ below which even two-dimensional waves are not expected to break. Yet, a significant number of them, some with steepness as low as $\epsilon = 0.03$ are detected as whitecapping. This is the subsiding (not breaking) phase, still detected as breaking if relied on whitecap observations. On the other end, out of two waves with $\epsilon \approx 0.27$, one wave does not exhibit whitecaps and another does, that is the first one is on its way up to the limiting steepness and another is on its way down while collapsing. This observations highlights uncertainties and ambiguity of existing definitions of breaking rates.

Finally, we would like to summarise main results, findings and conclusions of the numerical and laboratory investigations of the deep-water breaking in two-dimensional circumstances. Modulational-instability mechanism was found the driving force behind nonlinear evolution of steep waves, but it is not the cause of the breaking, as it may or may not lead to the breaking. The breaking will occur if the wave in the course of its nonlinear evolution reaches the limiting steepness, that is the water surface becomes unstable and collapses. Evolution of nonlinear wave properties was mainly investigated in the physical rather than Fourier space. Particular attention was paid to steepness, skewness and asymmetry of individual waves, and to their interplay leading to the breaking onset. Individual wave steepness was found to be the single parameter which determines whether the wave will break immediately, never break or take a finite number of wavelengths to break. Dimensionless distance to the breaking can be parameterised in terms of the wave steepness as the primary parameter. Properties of the incipient breaker were measured in detail.

If the wind forcing is superimposed, it can play multiple roles in affecting the wave-breaking dependences. Wind action is important on longer scales in altering breaking statistics because of enahcing the wave steepness. At moderate winds, doubling the wind speed leads to the limiting steepness and breaking four times as fast. At stronger wind forcing, this effect slows down. Instantaneously, wind capacity to affect the breaking onset is marginal unless the wind forcing is very strong.

Detailed laboratory observations revealed a number of additional features of the breaking process. At the breaking onset, wave period decreases (frequency increases) which further instigates the steepness growth towards the limiting state. Wave preceding the breaker is tilted backward and negatively skewed. Wave, following the breaker is transient. Its steepness, skewness, asymmetry and frequency are all growing, and it breaks soon after the first breaker (double-breaking). Features of the shape of the three waves appear to be inter-connected, particularly as the breaking onset is approaching, which fact indicates strong and rapid nonlinear interactions in the system. At the breaking onset, upshift of the spectral energy takes place. After the breaking, downshifting occurs. Superimposed wind influences the wave modulation and breaking severity. Strong wind makes the breaking more frequent, but smoothens the modulation, cancels the double-breaking and reduces the breaking strength. As a result, it affects the total dissipation in an unknown way. This very important issue needs further research.

Nature of breaking process, resulted from the nonlinear evolution and from the coalescing linear waves, is essentially different. While the limiting steepness of $\epsilon = ak = Hk/2 = 0.44$ appears to be the same in both cases, energy loss and distribution of this loss across the spectrum are completely dissimilar. This conclusion implies significant consequences for wave dissipation studies: i.e. research of the breaking and the dissipation have to be separated. While any process which leads to the critical steepness will cause the wave collapse, their end result in terms of the spectral dissipation will have principle differences. In other words, the breaking is in a way a kinematic effect (i.e. moving water surface becomes unstable, no matter what is a balance of forces other than gravity) whereas

the energy dissipation following the breaking is a dynamic process which remembers the history (i.e. depends on the driving forces both before and after the breaking onset).

Significant number of features typical of ocean breaking waves was reproduced in this two-dimensional fully-nonlinear study which points out to the modulational instability as a likely mechanism active in the field, at least at the scale of dominant waves. Most important further research, however, is needed into the role of this mechanism in broad-band and three-dimensional wave fields, particularly at the shorter wave scales. Since there are theoretical and experimental indications that this mechanism can be suppressed if frequency and directional spectra are broad, nature of wave energy dissipation and breaking can be different in three-dimensional wave fields, particularly at smaller scales characterised by broader angular distributions.

Alex Babanin and Dmitry Chalikov conducted this research with the support of an RDS (Research Development Scheme) grant of the Swinburne University of Technology. The authors are thankful to Alastair Jenkins and Yulia Troitskaya for useful discussions.

REFERENCES

Agnon, Y., Babanin, A. V., Chalikov, D. & Young, I. R. 2005 Fine scale inhomogeneity of wind-wave energy input, skewness and asymmetry. *Geophys. Res. Lett.* **332**, L12603, doi:10.1029/2005GL022701

Alber, I.E. 1978 The effects of randomness on the stability of two-dimensional wavetrains. *Proc. R. Soc. London* **A363**, 525–546

Babanin, A. V. & Soloviev, Y. P. 1998 Variability of directional spectra of wind-generated waves, studied by means of wave staff arrays. *Marine & Freshwater Res.*, **49**, 89–101

Babanin, A. V. & Soloviev, Y. P. 1998 Field investigation of transformation of the wind wave frequency spectrum with fetch and the stage of development. *J. Phys. Oceanogr.*, **28**, 563–576

Babanin, A. V., Young, I. R. & Banner, M. L. 2001 Breaking probabilities for dominant surface waves on water of finite constant depth. *J. Geophys. Res.* **C106**, 11659–11676

Babanin, A. V. & Young, I. R. 2005 Two-phase behaviour of the spectral dissipation of wind waves. *Proc. Ocean Waves Measurements and Analysis*, 5th Int. Symp. WAVES2005, 3-7 July, 2005, Madrid, Spain, Eds. B. Edge and J.C. Santas, paper 51, 11p

Babanin, A. V., Chalikov, D., Young, I. R. & Savelyev, I. 2007b Predicting the breaking onset of surface water waves. *Geophys. Res. Lett.* **34**, L07605, doi:10.1029/2006GL029135

Babanin, A. V., Banner, M. L., Young, I. R. & Donelan, M. A. 2007a Wave follower measurements of the wind input spectral function. Part 3. Parameterization of the wind input enhancement due to wave breaking. *J. Phys. Oceanogr.*, **36**, doi: 10.1175/JPO3147.1

Benjamin, T. B. & Feir, J. E. 1967 The disintegration of wave trains in deep water. Part 1. Theory. *J. Fluid Mech.* **27**, 417–430

Brown, M. G. & Jensen, A. 2001 Experiments in focusing unidirectional water waves. *J. Geophys. Res.* **C106**, 16917–16928

Caulliez, G. 2002 Self-similarity of near-breaking short gravity wind waves. *Phys. Fluids* **14**, 2917–2920

Chalikov, D. & Sheinin, D. 1998 Direct modeling of one-dimensional nonlinear potential waves. In *Nonlinear Ocean Waves*, Ed. Perrie W., Advances in Fluid Mechanics **17**, 207–258

Chalikov, D 2005 Statistical properties of nonlinear one-dimensional wave fields. *Nonlinear Processes in Geophys.* **12**, 1–19

Chalikov, D. & Sheinin, D. 2005 Modeling extreme waves based on equations of potential flow with a free surface. *J. Comp. Phys.* **210**, 247–273

Chalikov, D 2007 Simulation of Benjamin-Feir instability and its consequences. *Phys. Fluids.* **19**, 1–

Craig, W. & Sulem, C. 1993 Numerical Simulation of Gravity Waves. *J. Comp. Phys.* **108**, 73–83

Crapper, G. D. 1957 An exact solution for progressive capillary waves of arbitrary amplitude. *J. Fluid Mech.* **96**, 417–445

Dold, J. W. & Peregrine, D. H. 1986 Water-wave modulation. *Proc. 20th Int. Conf. Coastal Eng.*, Taipei, ASCE, 163-175

Dold, J. W. 1992 An efficient surface-integral algorithm applied to unsteady gravity waves. *J. Comp. Phys.* **103**, 90–115

Donelan, M. A., Longuet-Higgins, M. S. & Turner, J. S. 1972 Whitecaps. *Nature*, **36**, 172–1688

Donelan, M. A., Babanin, A. V., Young, I. R. & Banner, M. L. 2006 Wave follower measurements of the wind input spectral function. Part 2. Parameterization of the wind input. *J. Phys. Oceanogr.*, **36**, 1672–1688

Gemmrich, J. R. & Farmer, D. M. 2004 Near-surface turbulence in the presence of breaking waves. *J. Phys. Oceanogr.* **34**, 1067–1086

Janssen, P. A. E. M. 2003 Nonlinear four-wave interaction and freak waves. *J. Phys. Oceanogr.* **33**, 863-884

Holthuijsen, L. H. & Herbers, T. H. C. 1986 Statistics of breaking waves observed as whitecaps in the open sea. *J. Phys. Oceanogr.* **16**, 290–297

Liu, P. C. & Babanin, A. V. 2004 Using wavelet spectrum analysis to resolve breaking events in the wind wave time series. *Annales Geophysicae* **22**, 3335–3345

Longuet-Higgins, M. S. 1969 On wave breaking and equilibrium spectrum of wind-generated waves. *Proc. Rpy. Soc.* **A310**, 151–159

Longuet-Higgins, M. S. & Cokelet, E. D. 1976 The deformation of steep surface waves on water. I. A numerical method of computation. *Proc. R. Soc. Lond.* **A350**, 1–26

Longuet-Higgins, M. S. & Fox, M. G. H. 1977 Theory of the almost highest wave: The inner solution. *J. Fluid Mech.* **80**, 721–741

Longuet-Higgins, M. S. & Cokelet, E. D. 1978 The deformation of steep surface waves on water. II. Growth of normal-mode instabilities. *Proc. R. Soc. Lond.* **A364**, 1–28

Longuet-Higgins, M. S. & Dommermuth, D. G. 1997 Crest instabilities of gravity waves. Part 3. Nonlinear decelopment and breaking. *J. Fluid Mech.* **336**, 33–50

Manasseh, R., Babanin, A. V., Forbes, C., Rickards, K., Bobevski, I. & Ooi, A. 2006 Passive acoustic determination of wave-breaking events and their severity across the spectrum. *J. Atmos. Ocean. Technol.*, **23**, 599–618

Melville, W. K. 1982 Instability and breaking of deep-water waves. *J. Fluid Mech.* **115**, 165–185

Melville, W. K. & Matusov, P. 2002 Distribution of breaking waves at the ocean surface. *Nature* **417**, 58–63

Meza, E., Zhang, J. & Seymour, R. J. 2000 Free-wave energy dissipation in experimental breaking waves. *J. Phys. Oceanogr.* **30**, 2404–2418

Onorato, M., Osborne, A. R., Serio, M. & Bertone, S. 2001 Freak wave in random oceanic sea states. *Phys. Rev. Lett.* **86**, 5831–5834

Onorato, M., Osborne, A. R. & Serio, M. 2002 Extreme wave events in directional, random oceanic sea states. *Phys. Fluids* **14**, 25–28

Onorato, M., Cavaleri, L., Fouques, S., Gramstad, O., Janssen, P. A. E. M., Monbaliu, J., Osborne, A. R., Pakozdi, C., Serio, M., Stansberg, C. T., Toffoli, A., & Trulsen, K. 2008 Statistical properties of mechanically generated surface gravity waves: a laboratory experiment in a 3D wave basin. *J. Fluid Mech.*, submitted

Rapp, R. J. & Melville, W. K. 1990 Laboratory measurements of deep-water breaking waves. *Phil. Trans. R. Soc. Lond.* **A311**, 735–800

Tulin, M.P., & Waseda, T. 1999 Laboratory observations of wave group evolution, including breaking effects. *J. Fluid Mech.* **378**, 197–232

Waseda, T., Kinoshita, T. & Tamura H. 2008 Evolution of a random directional wave and freak wave occurrence. *J. Phys. Oceanogr.*, in press

Watson, K. M. & West B. J. 1975 A transport-equation description of nonlinear ocean surface wave interactions. *J. Fluid Mech.* **70**, 815–826

West, B. J., Brueckner, K. A. & Janda R. S. 1987 A new numerical method for surface hydrodynamics. *J. Geophys. Res.* **C92**, 11803–11824

Young, I. R. & Babanin, A. V. 2006 Spectral distribution of energy dissipation of wind-generated waves due to dominant wave breaking. *J. Phys. Oceanogr.* **36**, 376–394

Zaslavskii, G. M. & Sharkov, E. A. 1987 Fractal features in breaking wave areas on sea surface. *Doklady Academii Nauk SSSR (Transactions of USSR Academy of Sciences - English Translation)* **294**, 1362–1366

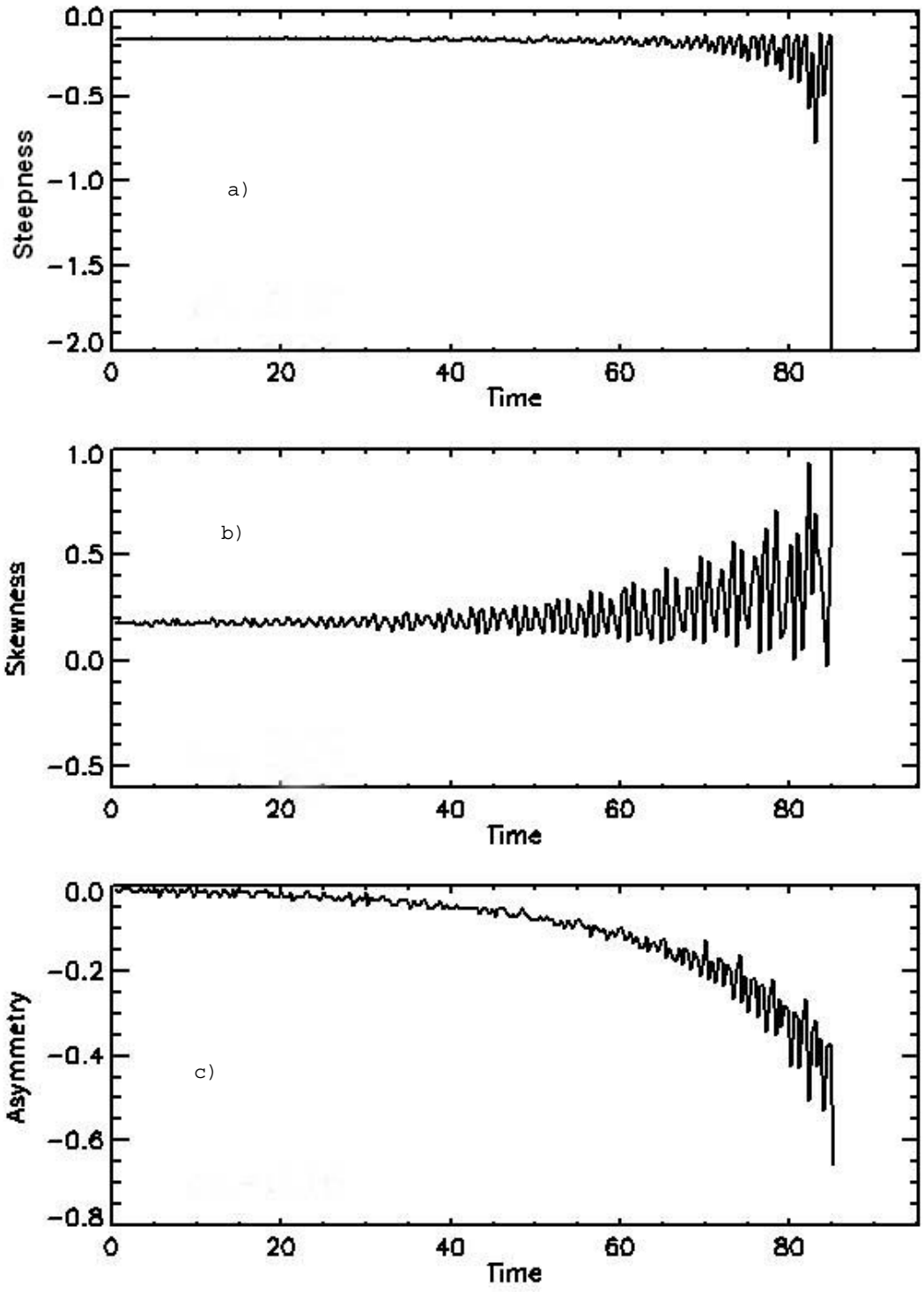
Steepness
0.0
−0.5
−1.0
−1.5
−2.0
a)
0
20
40
60
80
Time
Skewness
1.0
0.5
0.0
−0.5
b)
0
20
40
60
80
Time
Asymmetry
0.0
−0.2
−0.4
−0.6
−0.8
c)
0
20
40
60
80
Time